ISSN 0024-4902, Lithology and Mineral Resources, 2010, Vol. 45, No. 6, pp. 532–554. © Pleiades Publishing, Inc., 2010.
Original Russian Text © N.P. Chamov, S.Yu. Sokolov, V.V. Kostyleva, V.N. Efimov, A.A. Peive, G.N. Aleksandrova, M.E. Bylinskaya, E.P. Radionova, and S.I. Stupin, 2010, published in Litologiya i Poleznye Iskopaemye, 2010, No. 6, pp. 594–619.

Structure and Composition of the Sedimentary Cover in the Knipovich Rift Valley and Molloy Deep (Norwegian–Greenland Basin)

N. P. Chamov, S. Yu. Sokolov, V. V. Kostyleva, V. N. Efimov, A. A. Peive, G. N. Aleksandrova, M. E. Bylinskaya, E. P. Radionova, and S. I. Stupin

Geological Institute, Russian Academy of Sciences, Pyzhevskii per. 7, 119017 Russia
e-mail: nchamov@yandex.ru, sysokolov@yandex.ru

Received April 12, 2010

Abstract—The multidisciplinary approach is used to analyze the structure of the sedimentary cover in the northern Knipovich Rift valley, Molloy Fracture Zone and synonymous basin, Svyatogor and Hovgard rises, Gorynych Hills, Litvin and Pogrebitskii seamounts, and western slope of the Spitsbergen Archipelago studied in Cruise 24 of the R/V *Akademik Nikolaj Strakhov.* Materials of the bathymetric survey with multibeam echo sounder, as well as continuous seismic and vertical acoustic profiling, revealed two main (NNW- and NNE-trending) systems of fractures in the neotectonic structure of the region. It was established that a system of NNE-oriented fractures, linear zones of the dominant development of keyboard deformations included, is consistent with the strike of magnetic anomalies reconstructed for this region. Tectonic aspects of the Knipovich Rift and prospects of its further development are considered. Based on the wave field pattern of continuous seismic profiling (CSP) records, four seismocomplexes indicating contrasting sedimentation settings and intense tectonic processes at different formation stages of the northern Norwegian–Greenland Sea are conditionally defined in the sedimentary cover of the study region. It was established the Molloy Fracture Zone is responsible for a system of horizontal reflectors of acoustically transparent structureless light spots ("blankings") in the upper well-stratified part of the sedimentary section, which are characteristic of areas with ascending pore fluids. The micropaleontological study (palynomorphs of higher plants, dinocysts, planktonic foraminifers, and diatoms) revealed the presence of Miocene assemblages in sediments. Benthic foraminifers include late Paleocene–middle Eocene assemblages. The composition of rock-forming components demonstrates a directed succession of mineral–terrigenous associations from the feldspar–quartz type to mesomictic quartz–graywacke type.

DOI: 10.1134/S0024490210060039

Cruise 24 of the R/V *Akademik Nikolaj Strakhov* was dedicated to the study of the northern Knipovich Rift valley, Molloy Fracture Zone and synonymous basin, Svyatogor and Hovgard rises, Gorynych Hills, Litvin and Pogrebitskii seamounts, and western slope and shelf of the Svalbard Archipelago (Zaionchek et al., 2007, 2010).

These studies were conducted under the project "Late Mesozoic–Cenozoic tectonomagmatic evolution of the Barents Sea shelf and continental slope as a key to paleogeodynamic reconstructions in the Arctic Ocean" (A.V. Zaionchek and H. Brekke, supervisors) supported by the Norwegian Petroleum Directorate and programs of basic research nos. 14, 16, and 17 of the Presidium of the Russian Academy of Sciences (academicians G.A. Zherebtsov, V.M. Kotlyakov, N.P. Laverov, Yu.G. Leonov, and Yu.M. Pushcharovsky, supervisors).

In the Norwegian–Greenland Sea, the study area represents a link between structures of the Atlantic and Arctic oceans. This area is of key significance for understanding geological development of the entire Arctic region.

Extension and formation of sedimentary basins in Norway and eastern Greenland took place beginning from the Late Devonian–Carboniferous (Braathen et al., 2002; Eide et al., 2002; Hartz et al., 2002; Osmundsen et al., 2002, 2003).

Rifting in response to the Greenland–Laurentia left-lateral displacement relative to Baltica (Ziegler, 1988) resulted in multiple extension of the continental crust in Norway and stimulated the formation of numerous sedimentary basins above systems of normal faults degrading in the plastic zone of the middle crust (Mosar et al., 2002). According to reconstructions of the Greenland motion relative to stationary Europe (Torsvik et al., 2001), the most active phase of the Norwegian–Greenland Basin opening was characteristic of the Eocene 55–33 Ma ago (24–13 magnetic anomalies). Opening of the northern part of this basin began approximately 33 Ma ago (anomaly 13), when Greenland and Eurasia were separated from each

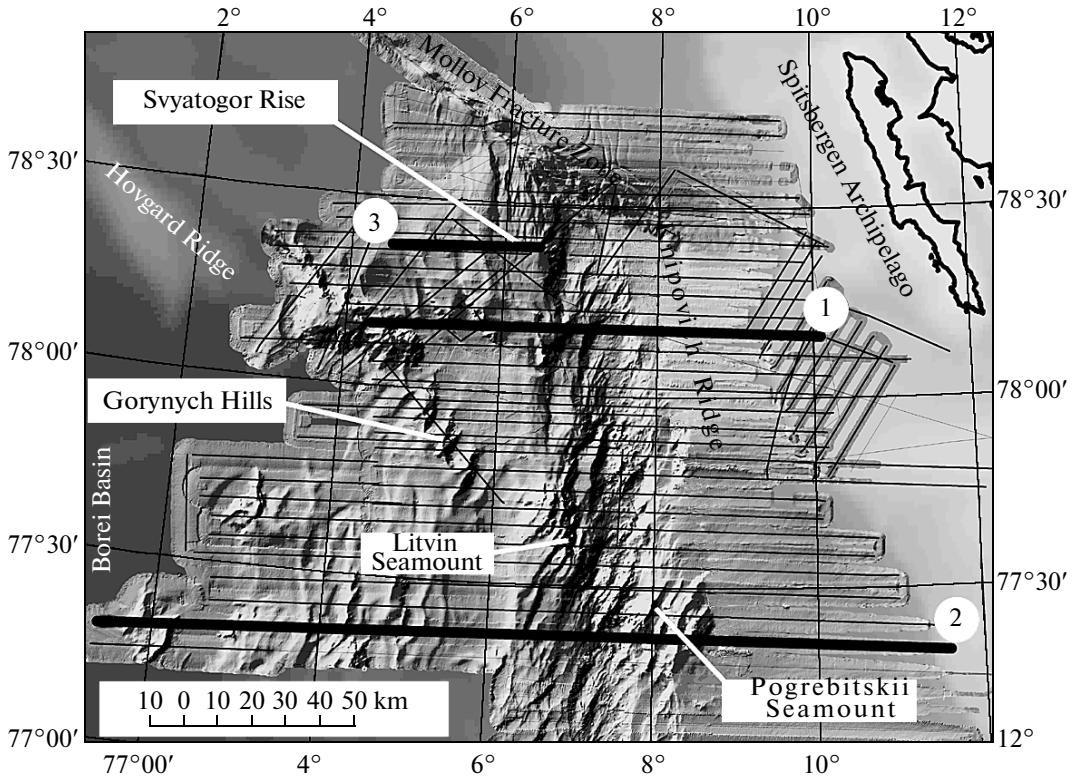

Fig. 1. Scheme of the study area in Cruise 24 of the R/V *Akademik Nikolaj Strakhov* (Geological Institute of the Russian Academy of Sciences, Norwegian Petroleum Directorate, 2006). The shaded relief was obtained by a SeaBat 8150 multibeam echo sounder (Zaionchek et al., 2007).

CSP profiles: (1) S24-P2-08, (2) S24-P2-22-3, (3) S24-P2-12b (fragment).

other (Talwani and Eldholm, 1977; Myhre et al., 1982).

Partial models for different rifting stages are considered in (Vogt, 1986; Torske and Prestvik, 1991; Parker, 1993; Lundin and Dore, 1997; Dore et al., 1999; Fleet and Boldy, 1999; Brekke, 2000; *Dynamics...*, 2000; Skogseid et al., 2000; Brekke et al., 2001).

Despite great attention of geologists to the study region, many aspects of its evolution remain debatable. For example, there is no common opinion so far about the nature of the Knipovich Rift, its formation time, and role in geodynamic development of the region.

The study of the sedimentary cover structure for defining its formation stages and sedimentation settings was one of the main purposes of the expedition. During the cruise, research profiles were oriented in the near-latitudinal direction in the area between 2° and 10°E and involved main morphostructures of the region: continental slope west of Spitsbergen, Knipovich Rift valley and westward uplifts, and, in particular, Hovgard Ridge, a presumable relict of the continental crust (Fig. 1). In the meridional direction, the study area extends from 79°04′N to 77°15′N and occupies the junction of the Molloy Deep and synonymous fracture zone with the northern segment of the Knipovich Ridge.

The article is dedicated to discussion of new data on the structure and age of the sedimentary cover based on the analysis of seismic profiling materials and sedimentary rocks dredged from the oceanic bottom.

METHODS

The bottom surface was studied using a SeaBat hydroacoustic complex (Reson Company, Denmark) that includes the deepwater (SeaBat 8150) and shallow-water (SeaBat 8111) echo sounders with the sonar function integrated with an EdgeTech 3300 profilograph and Octans orientation system, sound velocity sensor near antennas of echo sounders (SVP-70), and external sensor for measuring sound velocity in the water column (SVP-24). The data were accumulated and processed using a PDS 2000 (Denmark), SonarWiz (United States), and RadExPro 3.7 (Russia) software package.

The upper part of the sedimentary cover was studied by the vertical acoustic profiling (VAP) method using an EdgeTech 3300 nonparametric profilograph (United States) assigned for investigation of the upper part of the sedimentary cover to depths of 50–100 mbsf

at frequencies of 2–6 kHz and characterized by resolution of 0.15 to 1.0 m. For primary visualization, an EdgeTech base program was used. Initial files obtained during the acoustic survey were transformed into the SEGY seismic format using the program developed by S.Yu. Sokolov.

The sedimentary cover overlying the acoustic basement was studied with mapping of its acoustic stratification and tectonic deformations by the CSP method using original PSK-75 towed pneumatic gun (Efimov, 2009) with the size of working chambers of 0.5 and 10l. During the survey, the average effective reflecting area of neighboring profiles was characterized by overlapping of 87%, which yielded satisfactory correlation of the sedimentary cover at the central signal frequency of approximately 70 Hz.

The mineral composition of rock-forming clastogenic components in sandstones was determined in the Laboratory of the Comparative Analysis of Sedimentary Basins (GIN RAN) in line with the classification of sedimentary rocks by (Shutov, 1975). For the analysis, rock samples with fresh surfaces and without ice-rafting features were selected.

Microfossils were studied in laboratories of Paleofloristics, Quaternary Stratigraphy, and Micropaleontology (GIN RAN) by G.N. Aleksandrova (spores, pollen, dinocysts), M.E. Bylinskaya (Neogene foraminifers), E.P. Radionova (diatoms), and S.I. Stupin (Paleogene foraminifers).

CHARACTERISTIC OF THE MAIN MORPHOSTRUCTURES IN THE STUDY AREA

Development of numerous structures characterized by variable orientation, origin, and age reflects the complex and multistage destruction of the continental crust in the Norwegian–Greenland Basin (Fig. 2).

The *Molloy Deep* is a rhomboid in plane view. It is located at the southern termination of a relatively short synonymous spreading ridge, which extends in the northeastern direction up to the Spitsbergen Fracture Zone. The Molloy Deep represents the most subsided structure in the study area with water depths up to 5000 m and high (more than 2 km) and steep (20°–30°) slopes. The bottom topography of the basin is complicated by faults, landslides, and, likely, canyons (on the southern slope). The northern slope of the basin is bordered by two oval dome-shaped uplifts (Baturin, 1992).

The *Molloy Fracture Zone* governs the relative displacement of the Knipovich Rift valley and synonymous spreading ridge. In addition, the zone serves as a structural boundary of the Spitsbergen (northeastern side) and Greenland–Spitsbergen (southwestern) plateaus.

Along the strike (approximately 315°), the fracture zone exhibits its stepwise subsidence from the depth of 2200 m near its contact with the Knipovich Rift valley to 3000 m toward the Molloy Deep. Its walls are complicated by transverse faults. As a whole, the Molloy Fracture Zone represents a complex shear zone with the right-lateral component of shear movements, according to the localization of epicenters of recent earthquakes (Savostin and Karasik, 1981).

The *Greenland–Spitsbergen Plateau* is sandwiched between the Molloy Fracture Zone and Hovgard Ridge system. In the bottom topography, the plateau represents a slightly inclined structure, which extends in the northwestern direction toward the Greenland continental zone. The plateau retains its width (64–65 km) over its entire length. The eastern margin of the plateau hosts the Svyatogor Rise with the summit crest extending in the near-meridional direction. The latter structure is asymmetrical: its western slopes dip gradually toward the Greenland–Norwegian Plateau, while the eastern part of the rise exhibits a stepped faulted relief. As a whole, orientation of second-order structures in the Svyatogor Rise is governed by the closure and rotation of the Knipovich Rift valley at its junction with the Molloy Fracture Zone.

The Greenland–Spitsbergen Plateau and adjacent aseismic Hovgard Ridge, which is considered a relict of the thinned continental crust based on the geological–geophysical features, represent fragments of the previously common Cimmerian Greenland–Spitsbergen mobile belt, which was involved into the oceanic crust formation (Gusev, 1999).

We sampled only the southeastern segment of the ridge ("Hovgard Rise") that includes structures crosscut by transverse factures and a common base with the strike of approximately 315° and minimal water depth of about 1300 m.

Two large positive morphostructures (Gorynych Hills and Litvin Seamount) were mapped and sampled by dredging at the southeastern continuation of the Hovgard Rise. The Gorynych Hills comprise three en echelon linear rises extended in the meridional direction. They are situated on a common base oriented in the NW–SE direction. Like the Hovgard Ridge, some scarps of this system are characterized by the northeastern strike. The Litvin Seamount is a cone-shaped edifice with its summit located at a depth of 900 m.

The linear arrangement of the above-mentioned structures and their confinement to the southwestern boundary of the Greenland–Spitsbergen Plateau suggest that the plateau is a single lineament. This structure likely also includes the Pogrebitskii Seamount (located east of the Knipovich Rift valley) that comprises several en echelon linear NE-trending rises.

The *Knipovich Rift* is the main neotectonic structure of the study area. It extends over 550 km and adjoins the Molloy Fracture Zone in north and the Mohn spreading ridge in south.

In the study area, the rift is characterized by the near-meridional strike and well-expressed valley approximately 15 km wide and 2800–3400 m deep.

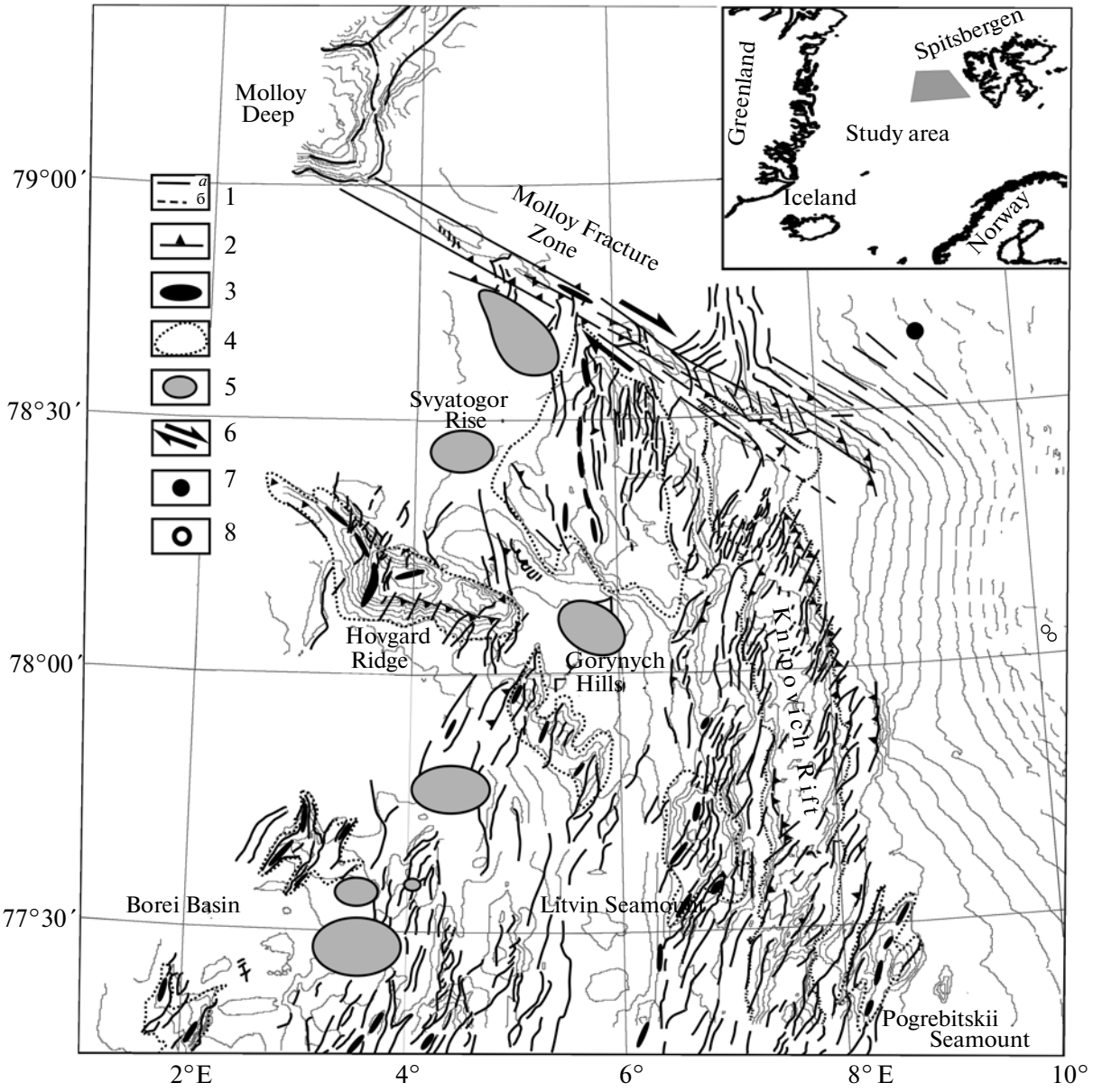

Fig. 2. Schematic tectonic structure of the northern Knipovich Ridge. Modified after (Peive and Chamov, 2008). (1) Faults (largely strike-slip faults): (*a*) observed, (*b*) assumed; (2) normal faults and downdip–strike-slip faults; (3) strike of principal positive structures; (4) contours of principal morphostructures; (5) areas with the dominant distribution of keyboard deformations (6) direction of movements along strike-slip faults; (7, 8) dislocations in the sedimentary cover presumably related to the fluid discharge: (7) the central-type edifice, (8) subsidence areas.

The bottom of the rift valley is represented by a system of en echelon depressions separated by NE-extended rises. It comprises four large pull-apart basins with their bottoms located at different hypsometric levels (Zaionchek et al., 2007, 2010).

The rift valley hosts numerous rises, some of which are active volcanoes with lava flows recorded by the sonar survey (Crane et al., 2001; Okino et al., 2002). The rift valley is characterized by the V-shaped transverse profile with the inclination of western and eastern slopes varying along the valley strike.

At its junction with the Molloy Fracture Zone, the rift valley is located at the shortest distance from the Spitsbergen Archipelago.

The eastern wall of the valley is relatively gentle, locally complicated by a system of scarps, and grades into the slope of the Spitsbergen Archipelago. The steep western slope is complicated by numerous scarps displaced relative to each other both along the strike and vertical direction.

Approximately 80 km west of the rift valley axis, the area includes a deep depression (Borei Basin) with

water depth exceeding 3000 m. It hosts two small rises with steep eastern and gentle western slopes and minimal water depths of 2200 and 2400 m, respectively. The morphology of these structures is scrutinized in (Peive and Chamov, 2008; Zaionchek et al., 2010).

SEDIMENTARY COVER STRUCTURE BASED ON THE CONTINUOUS SEISMIC AND ACOUSTIC PROFILING

The major part of the study area, where the CSP method revealed the acoustic basement surface, thickness of the sedimentary cover varies from zero to 700 m depending on particular morphological structures. On the western slope of Spitsbergen, thickness of the sedimentary cover could not be determined because of an insufficient power of the acoustic wave source.

Based on the wave field pattern in seismic records, we can divide the sedimentary cover into several seismocomplexes (Figs. 3, 4).

Seismocomplex A with a distinct upper boundary is confined to the continental slope. Since thickness of sediments exceeds the possibility of the CSP method, we could not define the acoustic basement in the area between the shelf edge and eastern wall of the Knipovich Rift valley (Fig. 3).

The sediments are well stratified with nearly parallel and wavy bedding. They are traced down to a few hundred meters by the CSP method and down to approximately 75 mbsf by the VAP method (Fig. 4a). Both remote methods revealed the development of unconformities and variations in the thickness of individual layers due to both variations in the sedimentation regime and deformations of sediments by slumping and tectonic processes. The reflection dynamics of the seismocomplex under consideration is high, which is documented by both CSP and VAP methods (Figs. 3, 4, respectively). In addition, the sedimentary section of this area is characterized by substantially shallower penetration of waves than in the abyssal part and on flanks of the ridge. The middle part of the slope exhibits numerous near-vertical tectonic fractures, which crosscut the entire sedimentary sequence. The continental slope section is characterized by the presence of acoustically transparent members of slump sediments.

Seismocomplex B is distributed virtually over the entire study area. The seismocomplex is missing only on steep fault-related slopes and largely defined by the VAP method.

It is represented by a thin (1–5 m) alternation of acoustically contrasting dark and light beds that are likely composed of the dominant clayey and sandy sediments. The seismocomplex is usually 20–25 m thick and as much as 80–100 m in depressions of the Borei Basin (Fig. 3b).

The presence of distinct reflectors, which can be traced over significant distances, indicates the formation of the seismocomplex during a tectonically passive sedimentation phase. In the present-day structure, distinct reflectors repeat the relief in areas of keyboard deformations. In areas with the development of normal faults, they extend parallel to fault planes and lack the fan-shaped divergence of layers typical of syntectonic sedimentation, for example, at the northeastern flank of the Hovgard Ridge (Fig. 4). This fact implies that the seismocomplex is older than the neotectonic structural pattern of the area. The sole exception is the wedge-shaped layers observed west of the Hovgard Ridge spur (Fig. 4b).

In the Molloy Fracture Zone area, Seismocomplex B is characterized by a system of horizontal reflectors of different-size (acoustically transparent) structureless light spots ("blankings"), which are governed by lower amplitudes of seismic waves in intervals of thinned fluid-saturated sediments. Small lenticular spots are usually oriented along bedding surfaces and locally defined in some beds as isolated structures (Fig. 4c). There are also larger rounded and vertically extended spots (up to 10–200 m along the long axis) that crosscut the bedding. One can see areas of thinned sediments and small anticlinal deformations that host the gaseous fluid migrating along near-vertical tectonic fractures, which are always associated with these structures and traced over tens of meters into the sedimentary section. The light-colored channels frequently connect the acoustically transparent lenses located at different hypsometric levels. They either disappear in the sedimentary sequence or reach the sea floor. Large channels confined to tectonic fractures look like near-vertical injection structures up to several tens of meters long (Fig. 4d).

The acoustically transparent and fault-line injection structures characterize the areas of pore fluid ascent (Ginsburg and Solov'ev, 1994; Valyaev, 1999). The tectonic compression regime required for realization of this process is emphasized by the development of distinct low-amplitude reverse faults (Fig. 4d). Data on the distribution of methane-bearing fluids and position of the bottom-simulating reflector (BSR) in the study area are given in (Vanneste et al., 2005; Chamov et al., 2008).

Seismocomplex C is characterized by a discrete distribution and more distinct acoustic stratification as compared with Seismocomplex D. We do not correlate it with the surface Seismocomplex B, which is also well stratified, although it is mapped only by the VAP method. The presence of a system of distinct reflectors to depths of 300–400 mbsf may be explained by the development of compact lithified sediments, average sedimentation rates, and availability of time for sediment compaction. Distribution areas of Seismocomplex C are lacking the acoustic basement with the morphology typical of oceanic basalts. Such basement has been detected only beneath Seismocomplex D. Samples of Seismocomplex C record are given in Figs. 4g and 4f.

Relation between seismocomplexes B and C depends on the particular geological structure. In

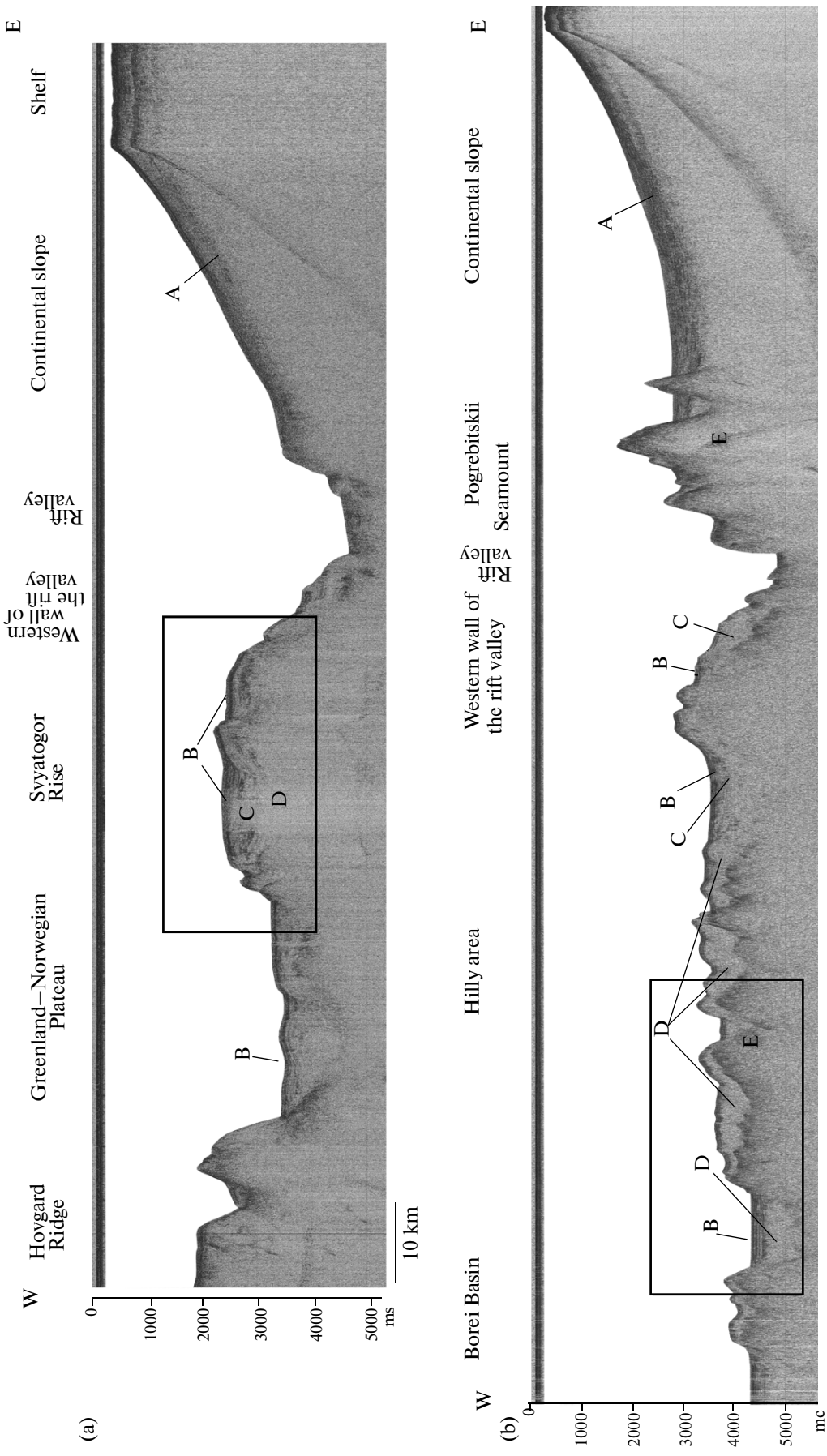

Fig. 3. CSP records along profiles: (a) S24-P2-08, (b) S24-P2-22. Boxes designate fragments presented in Figs. 4g, 4h. Letters in records are defined seismocomplexes. For the position of profiles, see Fig. 1.

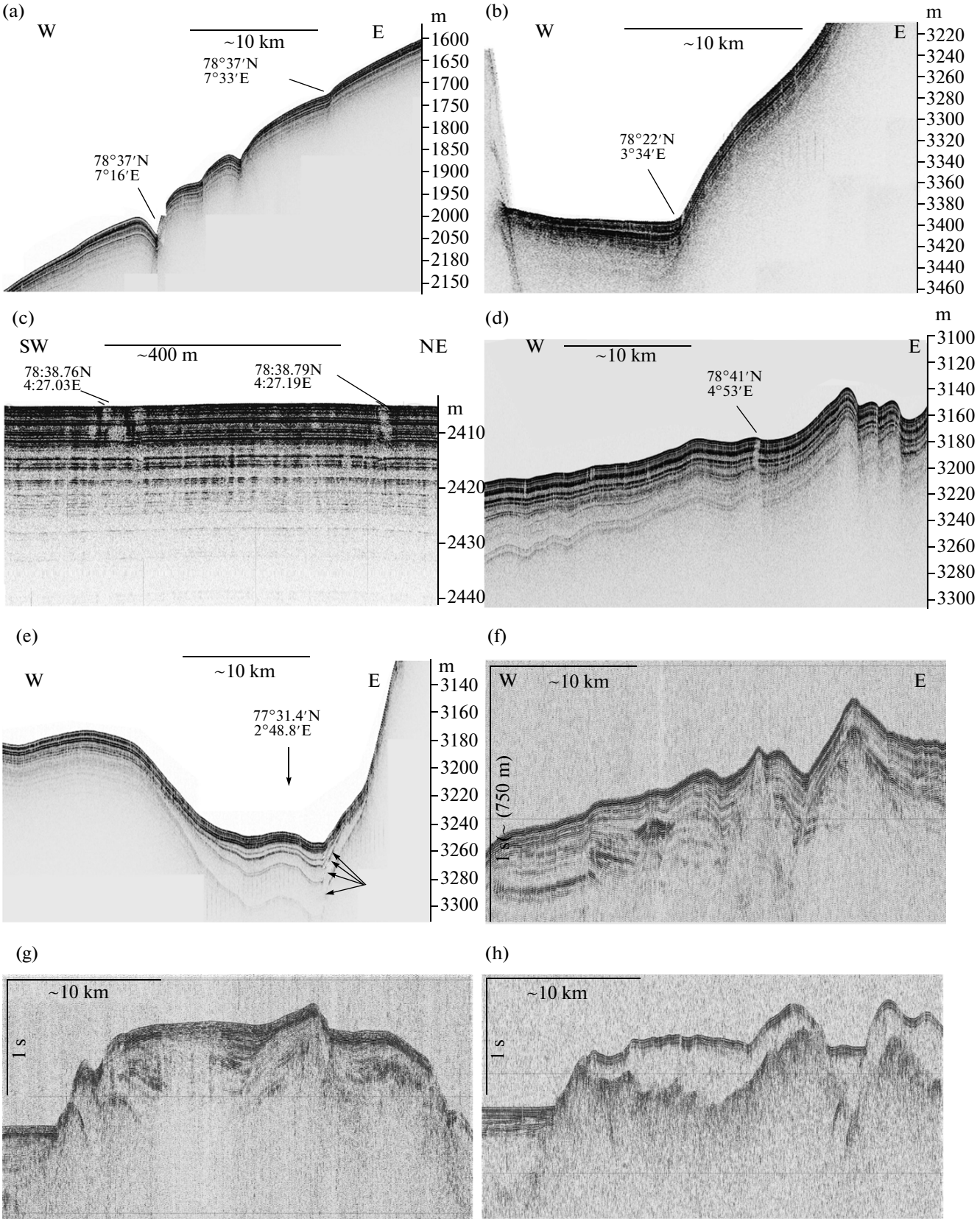
(a)
W
~10 km
E
m
78°37′N
7°33′E
78°37′N
7°16′E
1600
1650
1700
1750
1800
1850
1900
1950
2000
2050
2180
2150
(b)
W
~10 km
E
m
78°22′N
3°34′E
3220
3240
3260
3280
3300
3320
3340
3360
3380
3400
3420
3440
3460
(c)
SW
~400 m
NE
78:38.76N
4:27.03E
78:38.79N
4:27.19E
m
2410
2420
2430
2440
(d)
W
~10 km
E
m
78°41′N
4°53′E
3100
3120
3140
3160
3180
3200
3220
3240
3260
3280
3300
(e)
W
~10 km
E
m
77°31.4′N
2°48.8′E
3140
3160
3180
3200
3220
3240
3260
3280
3300
(f)
W
~10 km
E
1 s ~ (750 m)
(g)
~10 km
1 s
(h)
~10 km
1 s

Fig. 4. Characteristic wave field patterns. (a) Lower and middle parts of the continental slope; (b) wedge-shaped attitude of layers in the graben west of the Hovgard Ridge; (c) blanking areas in acoustic sections in the upper parts of sedimentary cover with horizontal beds; (d) low-amplitude reversed faults and light spots associated with anticlinal structures in sediments; (e) wedge-shaped attitude of beds in the upper part of Seismocomplex C (shown by arrows); (f) reflectors in Seismocomplex C (CSP S24-P2-12b profile, fragment); (g) record of Seismocomplex C (CSP S24-P2-08 profile, fragment); (h) record of Seismocomplex D (CSP S24-P2-22 profile). For the position of profiles, see Fig. 1.

areas without significant tectonic deformations, western slope of the Molloy Deep, and Greenland–Norwegian Plateau, the contact between seismocomplexes B and C is conformable (Fig. 4c). In other areas, it is characterized by wedge-shaped attitude of beds and angular unconformities (Figs. 4d, 4e).

Seismocomplex C is characterized by the development of inner unconformities and fan-shaped thickening of beds, which is primarily observed in asymmetric grabens (Figs. 4e–4g). The irregular bedding (often complicated by thickening) and the presumable sandy composition of sediments indicate high-energy hydrodynamics in sedimentation settings during intense tectonic movements.

In the Norwegian–Greenland Plateau area, the deepest reflector underlying Seismocomplex C is nearly horizontal and does not play a role of the acoustic basement of the oceanic type (Fig. 4f). Its thickness from the base of Seismocomplex B to strong reflectors is approximately 300 m. A similar reflector in the summit part of the Svyatogor Rise and on its western slope is located at a depth of approximately 400 and 200–250 mbsf, respectively (Figs. 3a, 4f, 4g).

Based on wave field patterns, *Seismocomplex D* is acoustically transparent and lacking internal reflectors. Its thickness is highly variable (Figs. 3b, 4h). Such sequences are usually related to avalanche sedimentation in middle parts of underwater fans with a high concentration of the coarse-detrital material. This is evident from the lack of contrasting reflectors that are usually characteristic of sequences with inner hiatuses, which emphasize difference between the compact underlying and the less lithified overlying sediments. The lack of a distinct upper surface and base (acoustic basement) in this seismocomplex suggests its high sedimentation rates. In other words, it is lacking features of normal pelagic sedimentation, which is accompanied by basement enveloping and near-horizontal bedding. At the same time, such sedimentary forms may be produced by the activity of bottom currents, which influence the accumulation (or reworking) of sedimentary material. They are known in areas influenced by contour currents in the Antarctic segment of the Atlantic Ocean (Sokolov et al., 1999).

The complete acoustic transparence likely suggests the largely sandy composition of sediments and their high accumulation rates, which decelerated lithification and provided the contrast between the underlying compacted and the overlying incoherent sediments. Such conditions are characteristic of avalanche sedimentation settings with the high influx of clastic material into an expanding accommodation space. The upper boundary of the seismocomplex in question (bottom or Seismocomplex B) is frequently indefinable. Its base coincides with the upper surface of the acoustic basement.

Let us note an interesting additional feature in the distribution of Seismocomplex D. Although its roof and base are dissimilar, it rests upon the basement almost horizontally. Similarity appears in areas characterized by a sharp rise of relief most likely due to crustal deformations, i.e., uplifting and inclination of small (3–5 km across) blocks. Such structures are observed in the hilly zone (Fig. 3b).

Seismocomplex E (acoustic basement) is readily distinguished over the major part of the study domain, except deep depressions, areas with thick sedimentary sequences on the eastern slope of the Knipovich Ridge, and fields of Seismocomplex C. It is characterized by specific reflections represented by a system of waves reflected from the rough basaltic surface of the second oceanic layer. The upper boundary of the seismocomplex is very contrasting due to a sharp jump of seismic wave velocities at the contact between sedimentary and igneous rocks. The seismocomplex is located at different depths relative to the sea level: 3000 m under depressions and 900 m in the Pogrebitskii Seamount area (Fig. 3b).

LITHOLOGY AND MICROFOSSIL ASSEMBLAGES

The characteristic of dredged rocks and their microfossil assemblages is given for observation stations shown in Fig. 5.

Station S2401: eastern slope of the Molloy Deep; starting dredging point: 79°04.77′N, 03°23.7′E, water depth 4523 m; terminal dredging point: 79°04.86′N, 03°27.41′E, water depth 3820 m.

The dredge recovered about 100 kg of mud (30%) and rocks (70%) represented by large blocks (50%) with uneven surfaces (up to 20 across) and small fragments (50%) approximately 4–5 cm in size. Lithological varieties include sandstones, siltstones, and mudstones (approximately 30, 10, and 55%, respectively). Exotic rock fragments likely represent the ice-rafted material (5%). Some rock fragments are covered by the ferromanganese crust up to 2 mm thick, whereas others fragments demonstrate features of tectonic deformations.

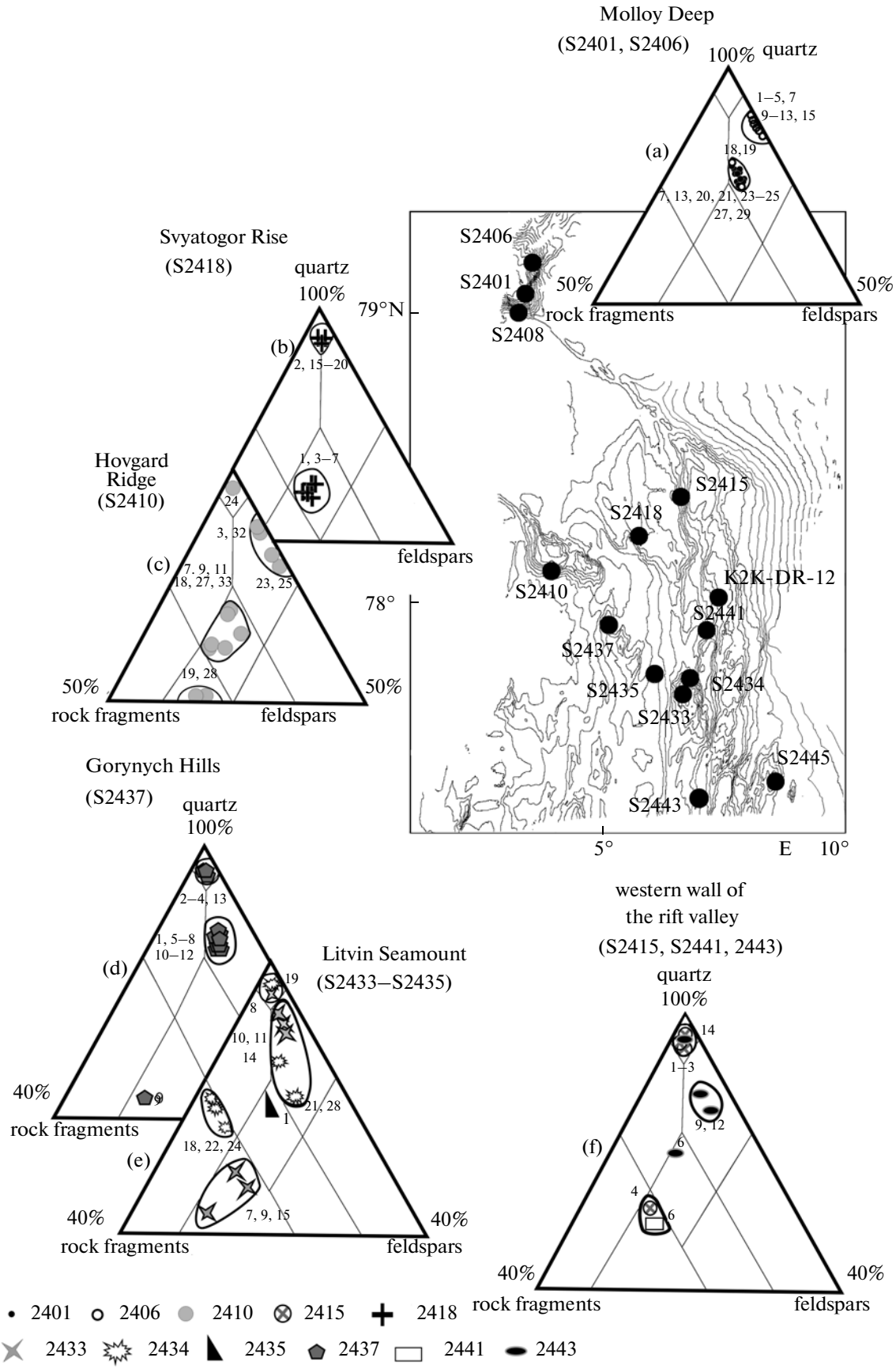
Molloy Deep
(S2401, S2406)
100% quartz
1–5, 7
9–13, 15
(a)
18,19
7, 13, 20, 21, 23–25
27, 29
50%
rock fragments
50%
feldspars
Svyatogor Rise
(S2418)
quartz
100%
(b)
2, 15–20
1, 3–7
feldspars
Hovgard
Ridge
(S2410)
24
3, 32
(c)
7, 9, 11
18, 27, 33
23, 25
19, 28
50%
rock fragments
50%
feldspars
S2406
S2401
S2408
79°N
78°
S2415
S2418
S2410
K2K-DR-12
S2441
S2437
S2435
S2434
S2433
S2445
S2443
5°
E
10°
Gorynych Hills
(S2437)
quartz
100%
2–4, 13
1, 5–8
10–12
(d)
Litvin Seamount
(S2433–S2435)
19
8
10, 11
14
40%
rock fragments
9
1
21, 28
18, 22, 24
(e)
7, 9, 15
40%
rock fragments
40%
feldspars
western wall of
the rift valley
(S2415, S2441, 2443)
quartz
100%
14
1–3
9, 12
(f)
6
4
6
40%
rock fragments
40%
feldspars
2401
2406
2410
2415
2418
2433
2434
2435
2437
2441
2443

Fig. 5. Positions of data points of the sandstone composition in the classification diagram by (Shutov, 1975). (a) Molloy Deep; (b) Svyatogor Rise; (c) Hovgard Ridge; (d) Gorynych Hills; (e) Litvin Seamount; (f) western slope of the rift valley. In the ternary diagrams, numerals designate sandstone sample numbers; figured symbols correspond to dredging stations.

Dredging stations: (S2401–S2445) R/V *Akademik Nikolaj Strakhov*; (K2K-DR-12 R/V *Professor Logatchev* (Gusev, 2005).

Sandstones (samples S2401/02–15, 20, 24, 25, 35) are gray, with local lenses of dark gray siltstone (sample S2401/20), calcareous laminates (sample S2422) and greenish gray volcanic (sample S2401/35) varieties included.

Siltstones (samples S2401/21, 23, 26, 33, 34, 36) are light gray to greenish gray and locally foliated (sample S2401/23).

Mudstones (samples S2401/16–19, 29–32, 36) are dark gray to black and massive, with laminated varieties (shales) and locally fissured.

Clays (samples S2401/1, 2) are moistened, dark gray and brown, with rare small mudstone inclusions.

Exotic rock material is represented by rounded fragments of gabbro-dolerite, quartzite, and granite.

Previous dredging on the western and southwestern slopes of the basin recovered ulltramafic rocks (Hansen et al., 2003).

Sample S2401/507 yielded a single test of the late Paleocene foraminiferal species *Subbotina* cf. *triloculinoides* (Plummer).

Station S2406: eastern slope of the Molloy Deep; starting dredging point: 79°10.63′N, 03°30.79′E, water depth 4590 m; terminal dredging point: 79°10.49′N, 03°41.13′E, water depth 3185 m.

The dredge recovered lithified clayey–sandy rocks (50%) and quartzite-type sandstones (45%) represented by fragments ranging from 1–2 to 20 cm in size. Ice-rafted material constitutes approximately 5%.

The clayey–sandy rocks are represented by greenish gray fine- to medium-grained thin-bedded silty sandstones, locally micaceous (samples S2406/1–8, 11–15) with clayey cement and dark gray to black mudstones. Most samples demonstrate distinct cleavage.

Silicified sandstones and gravelstones (samples S2406/9, 10, 16–19) are gray, fine- to medium-grained, massive, locally micaceous (sample S2406/10). Despite their general similarity, the rocks exhibit slight variations in density and silicification degree. The surface of some samples is cavernous and demonstrates boudinage features (Sample S2406/9). Slightly lithified light gray laminated (layers from 1–2 to 15 mm thick) sandstone of Sample S2406/16) contains small coalified detritus.

Exotic material is represented by six fragments of terrigenous rocks with smoothed surfaces.

Station S2408: southern slope of the Molloy Deep; starting dredging point: 79°02.80′N, 03°14.76′E, water depth 4939 m; terminal dredging point: 79°00.83′N, 03°12.07′E, water depth 3450 m.

The dredge recovered about 30 kg (25%) of rock fragments (3–5 to 13 cm across), clay rolls (2–4 cm in size) included, enclosed in compact mud (75%). The fragments are largely represented by sedimentary rocks: clays (50%), silty clays (45%), and ice-rafted material (5%).

The silty-clayey rocks include light gray silty–micaceous clays (samples S2408/2, 3) and dark gray carbonate-free clays (Sample S2408/501). Clays contain thin beds of laminated ferruginated siltstones, numerous fragments of white thin-walled molluscan shells, and fucoids. Sample S2408/1 encloses a cast (approximately 13 cm across) of the internal surface of the *molluscan* shell.

Silty varieties (samples S2408/4–8) are more compact and usually ferruginated. They occur as angular irregular fragments. Some samples demonstrate ferrugination along fissures.

There also fragments of dark gray laminated slightly lithified siltstone (sample S2408/503).

Exotic material is represented by several quartzite and silicified sandstone fragments up to 8 cm across.

Sample S2408/2 contains foraminifers: *Rhizammina* sp., *Karreriella horrida* Miatliuk), and *K. conversa* (Cushman). Their assemblage includes only agglutinated benthic species that likely inhabited depths below the carbonate compensation level.

Sample S2408/502 yielded two tests of planktonic foraminifers belonging to late Paleocene species *Subbotina* cf. *triloculinoides* (Plummer) and *Acarinina* cf. *subspherica* (Subbotina). Their reworking cannot be ruled out.

Sample S2408/2 contains palynomorphs. The palynological spectrum is dominated by poorly preserved bisaccate coniferous pollen: Disaccites, *Pinus* spp. Spores are rare and represented by species characteristic of Jurassic–Cretaceous rocks: *Leiotriletes, Todisporites* sp., *Biretisporites* sp., *Stereisporites* spp., *Deltoidospora* sp., *Cyathidites* sp., *Gleicheniidites* sp., *Lycopodiumsporites* sp., *Cicatricosporites* sp., *Osmundacidites* sp., *Foraminisporis asymmetricus* (Cookson et Dettman) Dettman, *F. wonthaggiensis* (Cookson et Dettman) Dettman, *Laevigatosporites ovatus* Wilson et Webster. They are accompanied by single pollen grains of *Triatriopollenites* sp., *T. plicoides, Alnus* sp., and *Tsuga* sp. characteristic of Eocene–Oligocene sediments.

The dinocyst assemblage includes different-age species: Early Cretaceous *Batioladinium micropodium*; Cretaceous *Exochosphaeridium phragmites* (Clarke et Verdier) Clarke et al., *Exochosphaeridium* sp., *Oligosphaeridium asterigerum* (Gocht) Davey et Williams;

Eocene–Oligocene *Wetzeliella* sp.; abundant Neogene *Barssidinium pliocenicum* (Head) Head, *Selenopemphix dionaecysta* Head et al., *S. brevispinosa* subsp. *brevispinosa* Head et al., *Reticulatosphaera actinocoronata* (Benedek) Bujak et Matsuoka; stratigraphically widespread *Spiniferites* sp., *Arteodinium* sp., *?Chytroesphaeridia* sp., *?Isabelidinium* sp. It also contains organic envelopes of microforaminifers.

The palynological spectrum from *sample S2408/3* is dominated by poorly preserved (indeterminable at the generic level) disaccate coniferous pollen (Disaccites). Spores and pollen complex is represented by different age taxa: Jurassic–Early Cretaceous *Stereisporites* spp., *Laevigatosporites ovatus*, *Osmundacidites* sp., *Verrucosisporites* sp., *Klukisporites* sp., *Neoraistrickia rotundiformis* (K.-M.) Taras., *Cicatricosisporites hallei* Delcourt et Sprumont, *Cicatricosisporites* sp., *Microreticulatisporites* sp., *Pilosisporites trichopapillosus* (Thiergart) Delcourt et Sprumont, *Murospora* sp., *Coprtospora paradoxa* (Cookson et Dettman) Dettman, *Perinopollenites elatoides* Couper, *Callialasporites dampieri* (Balme) Dev, *Classopolis* sp., *Inaperturpollenites limbatus* Balme, *Cerebropollenites mesozoicus* (Couper) Nillson, *Scyadopityspollenites macroverrucosus* (Their.) Iljina, *Quadriculina limbata* Mal., *Dipterella oblatinoides* Mal., *Podocarpidites* sp., Cycadaceae; Late Cretaceous–Early Paleogene *Deltoidospora* sp., *Gleicheniidites* spp., *Lycopodiumsporites marginatus* Singh, *Lycopodiumsporites* sp., *Taurocusporites reduncus* (Bolch.) Stover, *Trudopollis* sp., *Triatriopollenites* sp., *Rugubivesicullites* sp.; Eocene–Neogene *Jussiae* sp., *Tsuga* sp.; stratigraphically widespread *Leiotriletes* sp., *Cyathidites minor* Couper, Taxodiaceae–Cupressaceae, Pinaceae.

The dinocyst assemblage also consists of different-age taxa: Early Cretaceous *Batioladinium* sp.; Cretaceous *Chichaouadinium vestitum* (Brideaux) Bujak et Davies, *Circulodinium distinctum* (Deflandre et Cookson) Jansonius, *C.* cf. *attadalicum* (Cooks. et Eis.) Helby, *Circulodinium* sp., Exochosphaeridium sifidum *Exochosphaeridium* sp., *Odontochitina operculata* (O. Wetzel) Deflandre et Cookson, *Oligospheridium* asterigerum, O. *totum* Brideaux, *Chatangiella spectabilis* (Alberti) Lentin et Williams, *Chatangiella* sp., *Lejeunecysta* sp.; Eocene–Oligocene *Wetzeliella* sp.; Oligocene—Miocene *Selenopemphix selenoides* Benedek; stratigraphically widespred *Operculodinium* cf. *centrocarpum* (Deflandre et Cookson) Wall, *Hystrichosphaeridium tubiferum* (Ehrenberg) Deflandre, *Spiniferites* sp., *Apteodinium* sp., *?Chytroesphaeridia* sp., *Fibrocysta* sp., *Cribroperidinium* cf. *muderongense* (Cookson et Eisenack) Davey, *Isabelidinium* sp., *Microdinium ornatum* Cookson et Eisenack. The microfossil assemblage also includes acritarchs (*Paralecaniella indentata* (Deflandre et Cookson) Cookson et Eisenack, *Mycrhystridium* sp.), prasinophytes (*Leiosphaeridia* sp.), unidentifiable peridinioid cysts, and microforaminifera organic envelopes.

The spectrum from *sample S2408/5* is dominated by poorly preserved (indeterminable at the generic level) disaccate coniferous pollen (Disaccites). It is characterized by the mixed composition and includes different-age taxa: Jurassic–Early Cretaceous *Stereisporites* spp., *Cibotiumspora juncta* (Kara-Murza) Zhang, *Verrucosisporites* sp., *Osmundacidites* sp., *Foraminisporis Asymmetricus* Dett., *Cicatricosisporites* sp., *Lycopodiumsporites* sp., *Laevigatosporites ovatus* Wilson et Webster, *L. canalicus, Inaperturpollenites limbatus, Araucariacites australis* Cookson, *Quadriculina limbata* Mal., *Triatriopollenites plicoides* Zakl., *Alnus* sp., *Myrica* sp., *Alisprites* sp.; Eocene-Early Oligocene *Tricolpites* sp., *Triporollenites* spp., *T. plicoides* Zakl., *Alnus* sp., *Myrica* sp., Ericaceae; stratigraphically widespread *Leiotriletes* sp., *Cyathidites minor* Couper, and *Gleicheniidites* spp.

The dinocyst assemblage is also characterized by the mixed composition and largely represented by poorly preserved indeterminable chorate forms of the wide stratigraphic range: *Achomosphaera* sp., *Oligosphaeridium complex* (White) Davey et Williams, *Oligosphaeridum* sp. Stratigraphically significant taxa include Albian *Lithosphaeridium arundum* (Eisenack et Cookson) R.J. Davey, *Chichaouadinium vestitum*, Early Cretaceous *Pareodina* sp., *Subtilisphaera* sp., Late Cretaceous *Lejeunecysta* sp., *Surculosphaeridium* cf. *longifurcatum* (Firtion) Davey et al., and *Eocene–Oligocene Wetzeliella* species. There are also organic envelopes of microforaminifers and scolecodonts.

The mixed spore-and-pollen complex from *sample S2408/502* is composed of Jurassic–Cretaceous and Paleogene–Neogene taxa. The palynological spectrum is dominated by Paleocene–early Eocene pollen: *Aquilapollenites cruciformis* N. Mtchedlishvili, *Trudopollis* sp., *Triporopollenites robustus* Pfl., *Triporopollenites* spp., *Triatriopollenites plicoides* Zakl., *T. pseudorurensis* Pfl., *T. rurensis* Pflug et Thomson, *T. rorubituites* (Potonie) Pfl., and *Triatriopollenites* sp. They are accompanied by subordinate pollen of Eocene–Oligocene *Quercus* sp., *Comptonia* sp., *Carya* sp., *Juglans* sp., *Alnus* sp., *Myrica* sp., *Nuphar* sp., Ericaceae, Oligocene–Neogene *Compositae*, *Polygonium*, Jurassic–Early Cretaceous *Todisporites* sp., *Stereisporites* spp., *Polycingulatisporites* sp., *Cibotiumspora juncta*, *Kuylisporites lunaris* Cookson and Dettmann, *Osmundacidites* sp., *Foraminisporis wonthaggiensis, Klukisporites* sp., *Cicatricosisporites* sp., *Lycopodiumsporites* sp., *Laevigatosporites ovatus* Wilson et Webster, *L. canalicus, Classopolis* sp., *Inaperturpollenites limbatus, Quadriculina limbata* Mal., *Alisporites* sp., *Scyadopitys* sp., Late Cretaceous *Oculopollis* sp, stratigraphically widespread *Leiotriletes* sp., *Cyathidites australis* Couper, *C. minor* Couper, *Cyathidites* sp., *Gleicheniidites* spp., and coniferous pollen of *Cedripites* spp., *Podocarpidites* spp., *Pinus* spp. and poorly preserved Disaccites and Pinaceae grains indeterminable at the generic level.

The dinocyst assemblage is characterized by the mixed composition and represented by single specimens of Cretaceous (*Circulodinium* cf. *attadalicum*, *Odontochitina operculata*) taxa and species of a wide stratigraphic range (*Achomosphaera* sp., *Cribroperidinium* sp., *Impagidinium* sp., *Oligosphaeridium* sp.). Stratigraphically significant dinocysts are represented by Eocene–Oligocene (*Wetzeliella* sp.) and Neogene (*Selenopemphix dioneacysta, Selenopemphix* sp.) species.

General conclusion of the examination of palynomorphs. In all samples, spores, pollen, and dinocysts are characterized by the mixed composition. They include taxa of Jurassic, Cretaceous, Paleogene–Neogene ages and differ only by their proportions in particular assemblages. Such a composition is typical of Neogene–Quaternary sediments of the North Atlantic (Mudies, 1987, 1989; Head et al., 1989; Smelror, 1999). The dinocyst assemblages from the study area include *Selenopemphix dioneacysta*, the zonal middle Miocene form (de Verteuil and Norris, 1996) and characteristic Miocene taxa *Selenopemphix brevispinosa* subsp. *brevispinosa*, *Reticulatosphaera actinocoronata*, and *Barssidinium pliocenicum*, which are reported from upper Miocene sediments recovered by Hole 908 on the Hogvard Ridge (Pulsen et al., 1996) and Pliocene sediments from Hole 986D (seismic units SV-VIII and SV-VII) drilled in the western margin of Spitsbergen (Smelror, 1999). This fact provides grounds for dating samples obtained at Station S2408 as the late Miocene–Pliocene.

Sample S2408/502 also contains diatoms *Trinacria regina, T. exculpta* var. *tetragona* mostly characteristic of uppermost Paleocene–basal Eocene sediments, and *Nitzschia* sp. known beginning from the Miocene.

Station S2410: southern slope of the Hovgard Ridge; starting dredging point: 78°05.64′N, 03°53.48′E, water depth 2778 m; terminal dredging point: 78°07.25′N, 03°52.17′E, water depth 2224 m.

The dredge recovered fragments of lithified sedimentary rocks and large clayey lumps enclosed in a light brown mud. The total weight of fragments is 30 km (approximately 30% of the entire dredged material). The fragments 0.5–1.0 cm across (on average) are characterized by different degrees of roundness and smoothed edges. They are covered by a black compact ferromanganese crust.

The clays contain variably rounded and chaotically oriented pebbles of sedimentary rocks (samples S2410/1, S241034). Some fragments show traces of glacial scouring. The rock fragments are represented by carbonaceous and light gray mudstones (sample S2410/2), thin-bedded silty shales (sample S2410/4), light gray siltstones (samples S2410/5–8, 10, 14), silty sandstones (samples S2410/31, 32), fine- to medium-grained thin-bedded sandstones (samples S2410/3, 18–20, 30, 33), silicified sandstones (samples S2410/12, 13, 17, 21, 22, 27), and quartzites (samples S2410/23–25).

Some sandstone samples exhibit slumping (sample S2410/9), bioturbation (sample S2410/16), and brecciation (sample S2410/11) textures. Sample S2410/30 demonstrates two systems of laminae 1 to 2 mm thick (horizontal and cross-bedded). In addition, the rock collection includes single fragments of pinkish brown limestone (sample S2410/15) recrystallized up to the point of development of calcite, potassic granite approximately 2 cm across (sample S2410/29), and irregular iron hydroxide nodule approximately 4 cm in size (sample S2410/26). One can also see sponge spicules and well-preserved Pogonophora shells.

Station S2415: western slope of the Knipovich Rift valley; starting dredging point: 78°22.26′N, 06°44.94′E, water depth 3082 m; terminal dredging point: 78°21.85′N, 06°32.6′E, water depth 2015 m.

The dredge recovered about 50 kg of uniform viscous dark gray mud with rock fragments (about 5% of the whole material) 1–15 cm across (prevalent size 3–4 cm).

The fragments are represented by the dark gray compact massive quartz sandstones (samples S2415/1–3), greenish gray less compact thin-bedded sandstones (sample S2415/4), gray massive siltstones (sample S2415/5), gray compact (sample S2415/8) and black (sample S2415/6) locally silicified (sample S2415/8) mudstones, limestones, pinkish white quartzites (sample S2415/11), and quartz–chlorite schists (sample S2415/12). Some samples are covered by thin films of iron and manganese oxides. In sample S2415/10, the ferromanganese crust is 2 mm thick.

Station S2418: southwestern slope of the Svyatogor Rise; starting dredging point: 78°13.4′N, 05°37.34′E, water depth 1848 m; terminal dredging point: 78°13.58′N, 05°46.34′E, water depth 1543 m.

The dredge recovered about 70 kg (80%) of mud and 20 kg (20%) of compact clays and rock fragments of variable composition, size and roundness degree. The fragments are composed of unsilicified (about 50%) and silicified (about 40%) terrigenous rocks and ice-rafted material (10%). In addition, they include iron hydroxide nodules (sample S2418/12) and single hollow concretion partly filled with semiliquid clayey material (sample S2418/11).

Clays are represented by a compact grayish brown variety with rare inclusions of rounded fragments of carbonaceous mudstones and compact sedimentary rocks up to 1 cm across (samples S2418/21, 22) and less compact gray variety (sample S2418/23).

The unsilicified terrigenous rocks include rounded or less common angular sandstone (samples S2418/1–7) and mudstone (samples S2418/8, 9) fragments.

The sandstones are light gray to greenish gray, massive, thin- to irregularly bedded, fine- to medium-grained and inequigranular, with rare inclusions of plant detritus and mica that emphasize bedding surfaces (samples S2418/6 and 7). Sample S2418/10

demonstrates a contact between the fine-gained thin horizontally bedded sandstone and the dark gray shale.

The mudstones are represented by the brownish and dark gray carbonaceous thin-bedded (sample S2418/9) and foliated (sample S2418/8) varieties. Foliation surfaces are ferruginated.

Another group of rock fragments consists of silicified sandstones and mudstones. The size of angular fragments ranges from 1 to 20 cm (average 3–5 cm).

The sandstones are brownish gray, massive to horizontally laminated, and medium- to coarse-grained (samples S2418/5–9, 20). Most sandstone samples contain biotite (about 20%), which emphasizes the bedded rock structure. Sample S2418/9 exhibits small irregularly scattered sulfite inclusions.

The mudstones are dark gray, brecciated (sample S2418/13), and crosscut by a dense system of calcite veinlets.

Ice-rafted material is represented by the fragments of granite, diorite, granite-gneiss, dark gray limestone, light quartz sandstone, and mudstone. The sandstone fragment from sample S2418/3 demonstrates distinct glacial striation.

Station S2433: upper part of the eastern slope of the Litvin Seamount; starting dredging point: 77°40.87′N, 07°44.78′E, water depth 1250 m; terminal dredging point: 77°42.28′N, 07°39.84′E, water depth 952 m.

The dredge recovered about 70 kg of material: 30% of mud and 70% of rock fragments of variable lithology, size, and roundness degree. The fragments are dominated by terrigenous rocks (about 50%), basalts (40%), ice-rafted material (about 10%), and single clasts of carbonate rocks.

Mud is represented by the moistened plastic clays with abundant small light gray carbonate tubes resembling coral processes (calcareous sponges or algae?) (samples S2433/25, 36).

The basalt fragments (samples S2433/1–6) are composed of the aphyric and plagioclase porphyric (plagioclase crystals up to 0.5 cm long) varieties of pillow lavas. The fragments are characterized by the weathered surface (alteration zone up to 1 cm thick) and ferrugination along fissures. The rock includes particles of palagonitized volcanic glass up to 0.4 cm across.

Terrigenous rocks are represented by sandstones, siltstones, mudstones, and conglomerates.

The sandstones are gray, massive, and fine- to medium-grained (samples S2433/7, 8, 13, 14). Their vaguely bedded varieties (sample S2433/9) contain small detritus and large fragments (up to 1.5) of carbonaceous matter. Sample S2433/18 exhibits intercalations of darker silty material. There are also poorly lithified dark brown and brownish medium-grained ferruginated sandstones (samples S2433/10, 11) and rare light gray sandstone varieties with carbonate cement (sample S2433/12), which enclose bivalve, ostracod, and, presumably, gastropod shells. Some fragments are covered by ferromanganese crusts up to 5 mm thick.

The siltstones (samples S2433/17, 20, 22), silty mudstones (sample S2433/19), and mudstones (sample S2433/21) are dark brown, slightly micaceous, and massive.

The conglomerates (sample S2433/15) are crimson-brown, with well-rounded pebbles (0.5–1.5 cm across) and carbonate cement. They presumably originate from the Devonian Old Red Formation developed in Western Spitsbergen Island.

Carbonate mineralization is developed as of crusts (samples S2433/12, 23). Many rock fragments are encrusted with carbonate organisms, such as *Serpula, Nubecularia* (sample S2433/24) and carbonate sponges (?) (samples S2433/25, 26) as a tubular net.

Ice-rafted material includes fragments of coarse-grained gabbro, quartz–micaceous gneisses, granites, quartzites, and mudstones.

Station S2434: eastern slope of the Litvin Seamount; starting dredging point: 77°42.06′N, 07°01.65′E, water depth 2410 m; terminal dredging point: 77°42.28′N, 06°48.7′E, water depth 1402 m.

The dredge recovered about 100 kg of rock fragments (80%) and mud (20%), The rocks are represented by large fragments and angular clasts of altered basalts (40%), sandstones (35%), mudstones (10%), and ice-rafted material (15%).

Semiliquid muddy material consists of dark compact, viscous, vaguely bedded clays (sample S2434/36) with angular mudstone and siltstones fragments, quartz sandstone pebbles (from 1 m to a few centimeters in size), brownish gray slightly lithified carbonate sandstones with numerous fucoids (sample S2434/33), and dark gray to greenish gray compact but soft clayey siltstones (samples S2434/34, 35). All these rock varieties are characterized by obscure bedding and faunal fossils.

Basalts (samples S2434/1–15) are aphyric, vesicular, and more intensely weathered than their counterparts in dredge S2433. The fragments (5–15 to 40 cm) are angular with sectorial jointing and coated with iron and manganese hydroxides. They frequently display crusts of quenched volcanic glass, which is mostly palagonitized. Amygdules in basalts are locally filled with carbonate matter.

The sandstones are light gray (locally with yellowish tint) fine- to medium-grained (samples S2434/20–25, 28). The prevalent size of sandstone fragments is 3–10 cm. Most samples are covered by a thin ferromanganese crust. The rocks are characterized by discrete horizontal bedding and slumping (sample S2434/22). There are also lilac and cherry-crimson inequigranular massive sandstones with occasional gavel-sized inclusions (samples S2434/18, 19).

Siltstones are dark gray and thin-bedded (sample S2434/26). Mudstones are silty and slight lithified

(sample S2434/27). There are also subordinate calcareous varieties.

Exotic material is represented by gneisses, granites, quartz sandstones, quartzites, cherts, micaceous schists, dark gay pelitomorphic limestones, light gray cavernous brecciated limestones with carbonaceous fragments, and compact, vaguely bedded, calcareous sandstones with intercalations of ferruginated matter.

Sample S2434/35 yielded benthic foraminifers *Spirosigmoilinella* sp., *Glomospirella* sp. emend Miller et al., 1982, *Reticulophragmium amplectens* (Grzyb.), and *Lenticulina* sp. (for age, see Station S2441).

Station S2435: western slope of the Litvin Seamount; starting dredging point: 77°43.85′N, 06°33.24′E, water depth 1450 m; terminal dredging point: 77°43.31′N, 06°39.42′E, water depth 1067 m.

The dredge recovered about 150 kg of mud (95%), 10 angular and subangular (sandstone and limestone) fragments and ice-rafted material represented by granite-gneisses.

The sandstones are gray, horizontally laminated with coalified detritus along bedding surfaces (sample S2435/1).

Carbonate rocks are represented by dark gray pelitomorphic (sample S2435/2) and light gray organogenic-detrital (sample S2435/3) limestones with impressions of bivalve shells and corals at the weathered surface.

Station S2437: southeastern slope of the northern summit of the Gorynych Hills; starting dredging point: 77°54.84′N, 05°10.9′E, water depth 2500 m; terminal dredging point: 77°55.30′N, 05°08.65′E, water depth 2068 m.

The dredge recovered about 120 kg of viscous mud (30%) with pebbles and angular rock fragments represented by sedimentary sandy–clayey varieties (60%) and ice-rafted material (about 40%). Most fragments are covered partly by black ferromanganese crusts up to 2 cm thick (samples S2437/3–35).

The clayey rocks are represented by compact rusty yellow–ray nonuniform clay (sample S2437/31) with abundant sand-sized grains and dark brown carbonaceous silty clay (sample S2437/15). Semiliquid clayey material encloses rolls of compact ferruginated sandy clays, sandstones, ferruginous crusts of incoherent iron hydroxides (sample S2437/24), and single spheroid nodules of ferruginous material (samples S2437/22, 23).

The sandy–clayey varieties include sandstones (samples S2437/1–13, 28), siltstones (samples S2437/14, 17), mudstones, silty mudstones (samples S2437/16, 25–27), and aleuropelites (samples S2437/29, 30).

The sandstones are fine- to coarse-grained, compact to incoherent, with the ferruginous cement. The latter variety is characterized by the weathered crust up to 0.4 cm thick. One can see brown to brown gray massive micaceous sandstones with obscure horizontal bedding (samples S2437/1–6, 8, 9, 11, 28), light gray thin-platy fine-grained varieties with mica and carbonaceous detritus (sample S2437/7), sandstones with thin discrete bedding (sample S2437/13), and crimson-gray fine-grained massive sandstones with almost colorless quartz (sample S2437/10). Inequigranular sandstone from sample S2437/8 exhibits discrete horizontal bedding, small carbonaceous–clayey inclusions (0.3–0.7 cm across), and single pebbles (up to 2 cm in size) oriented along bedding. In samples S2437/9 and S2437/11, sandstones enclose discrete carbonaceous–clayey inclusions.

The siltstones are micaceous and intercalated with mudstones (samples S2437/14, 17). The latter sample exhibits faunal remains at the fresh surface.

The mudstones and silty mudstones are black to brown-black, compact, platy, with mineralization-free slickensides on the platy jointing surface (samples S2437/16, 25–27).

The aleuropelites are rusty-brown, calcareous, compact, massive, uniform, with inclusions of dark matter (samples S2437/29, 30).

Ice-rafted material includes biotite gneisses, granites, granodiorites, and sedimentary rocks: usually silicified sandstones, mudstones, organogenic-detrital and pelitomorphic silicified limestones. Limestone (sample S2437/18) contains brachiopods of the *Productus* group.

Station S2441: western slope of the Knipovich Rift valley; starting dredging point: 77°54.42′N, 07°12.82′E, water depth 2930 m; terminal dredging point: 77°54.22′N, 07°04.39′E, water depth 2140 m.

The dredge recovered about 300 kg of fragments of compact clays and terrigenous sedimentary rocks with fresh surfaces and plastic gray mud (about 10%).

The strongly compacted clays (15%) are structureless, calcareous, with pudding pebbles up to 3 cm across (samples S2441/1–3).

Sandstones (5%) are olive-green and brownish gray, compact, fine- to medium-grained (samples S2441/8–16). Some varieties are characterized by carbonate cement (sample S2441/12). Most sandstones are hydrothermally altered and ferruginated. Sample S2441/15 is crosscut by a dense system of quartz veinlets up to 2 mm thick.

Siltstones (30%) are light gray, horizontally laminated (samples S2441/4–7, 21, 22), platy, with small lenses and intercalations of light gray quartz sandstone (1–3 mm to 1 cm thick) and elongated bedding-parallel pebbles (clay rolls), small gravel-sized grains, and angular fragments (up to 1 cm across) of sandy rocks and, less commonly (sample S2441/6), strongly altered basalts.

Mudstones and silty mudstones (40%) are black, cross-laminated, platy, carbonate-free (samples S2441/17—20, 23). All samples demonstrate boudinage and slickensides.

Ice-rafted material is represented by rounded fragments and boulders of sandstone, quartzite, siltstone, and alkali gabbro.

Sample S2441/4 yielded planktonic foraminifers *Globorotalia opima nana/continuosa, Globigerinoides ruber.* and *G/ trilobus*. According to (Bolli and Saunders, 1985), the transitional form *nana/continuosa* existed in the Oligocene–early Miocene, Zone N6 included. *G. trilobus* and *G. ruber* appeared in the early Miocene (uppermost N4 and N5 zones, respectively). Thus, age of siltstone from sample S2441/4 likely corresponds to zones N5 and N6 of the standard scale (approximately middle–early Miocene, 17–20 Ma).

Benthic foraminifers indicating bathyal depths are identified in the following samples: sample S2441/6: *Reticulophragmium pauperum* (Chapman); sample S2441/19: *Cibicidoides alleni* (Plumm.); sample S2441/20: *Saccammina placenta* (Grzyb,), *Trochammina* sp. emend Gradstein et al., 1994; sample S2441/21: *Saccammina placenta* (Grzyb,), *Cibicides alleni* (Plumm.); sample S2441/22: *Saccammina placenta* (Grzyb,); sample S2441/23: *Ammomarginulina aubertae* Gradstein et Kaminski, *Clavulina* cf. *anglica* (Cush.), *Caudamina* cf. *excelsa* (Dylazanka).

This foraminiferal assemblage is dated back to the late Paleocene–middle Eocene based on its comparison with counterparts from the North Atlantic and West Arctic regions (Miller et al., 1982; Gradstein and Kaminski, 1989; Hulsbos et al., 1989; Boltovskoy et al., 1992; Gradstein et al., 1994; Nagy et al., 1997, 2000). This conclusion is also valid for the foraminiferal assemblage from sample S2434/35.

Dredging carried out in this area (starting dredging point: 77°50.97′N, 07°19.52′E; terminal dredging point: 77°50.99′N, 07°22.8′E) by a K2K-DR-12 dredge in the depth interval of 3480–2630 m during the cruise of the R/V *Professor Logatchev* yielded rock samples with the Oligocene assemblage of planktonic and benthic foraminifers (Gusev, 2005).

Thus, based on the analysis of smaller foraminifers, we can conclude that the western slope of the rift valley (the eastern slope of Litvin Seamount included) at stations S2434 and S2441 is composed of upper Paleocene–middle Miocene, Oligocene, and Miocene rocks.

Station S2443: western slope of the Knipovich Rift valley; starting dredging point: 77°15.45′N, 07°11.47′E, water depth 3052 m; terminal dredging point: 77°15.00′N, 07°08.00′E, water depth 2220 m.

The dredge recovered about 100 kg of large fragments terrigenous sandy–clayey rocks (30%), strongly altered basalts, rare volcanic glass (15%), black laminated ferromanganese crusts (40%), and ice-rafted material (15%).

Terrigenous rocks are represented by sandstones (samples S2443/5, 6, 13, 14), silty sandstones (samples S2443/7–10), siltstones (samples S2443/11, 12), and mudstones.

The sandstones are light gay and light brown, fine- to medium-grained, massive, discretely and thin-bedded, with inclusions of carbonaceous material. sample S2443/13 demonstrates alternation of gray compact silicified cross-bedded sandstone and brown thin-bedded silty sandstone.

The silty sandstones are rhythmically thin-bedded platy. They are accompanied by light gray and brown thin-bedded compact clayey siltstones and silty clays resembling carbonate-free compact clayey varieties from Station 2441.

The basalts are weathered, locally decomposed, rusty brown, aphyric (samples S5443/1, 2, 4) and plagioclase porphyric (sample S2443/3). The latter variety contains large phenocrysts (approximately 60% of the rock). Volcanic glass is completely palagonitized. The samples are usually covered by ferromanganese crusts up to 5 mm thick.

Ice-rafted fragments are usually rounded and presented by granites, silicified sandstones, gneisses, and siltstones.

Station S2445: southeastern slope of the Pogrebitskii Seamount; starting dredging point: 77°19.97′N, 08°56.29′E, water depth 2030 m; terminal dredging point: 77°20.99′N, 08°52.54′E, water depth 1590 m.

The dredge recovered about 200 kg of basalt and dolerite boulders and fragments (about 90%). The remaining part is composed of ice-rafted rocks (5%) and fragments of greenish gray compact calcareous clays with differently oriented slickensides (5%) (samples S2445/13–15, 20). They contain subordinate conglomerates with the carbonate cement (samples S2445/16, 17) and carbonate crusts (samples S2445/18, 19, 22).

The basalts are aphyric (samples S2445/1–8) and plagioclase porphyric (S2445/9–12) with sectorial jointing characteristic of lava flows. With respect to texture, sample S2445/12 is close to dolerite.

Some basalt samples are intensely weathered and covered by ocherous shelly ferromanganese crusts or chloritized. Only two samples contain the palagonitized glassy and quenched zones up to 0.5 cm thick (samples S2445/1, 2).

The exotic material is represented by fragments of quartzite, quartz sandstone, granite, and granite-gneiss.

LITHOGENETIC TYPES OF SANDY ROCKS

Figure 5 presents data on the rock-forming clastogenic components calculated in thin sections of sandstones dredged from the main morphological structures of the study area.

Based on all textural and compositional features of rocks (sorting, roundness degree, composition of rock-forming clastogenic components, and cement), we can divide the sandstones into the feldspar–quartz and mesomictic quartz–graywacke types (Fig. 6).

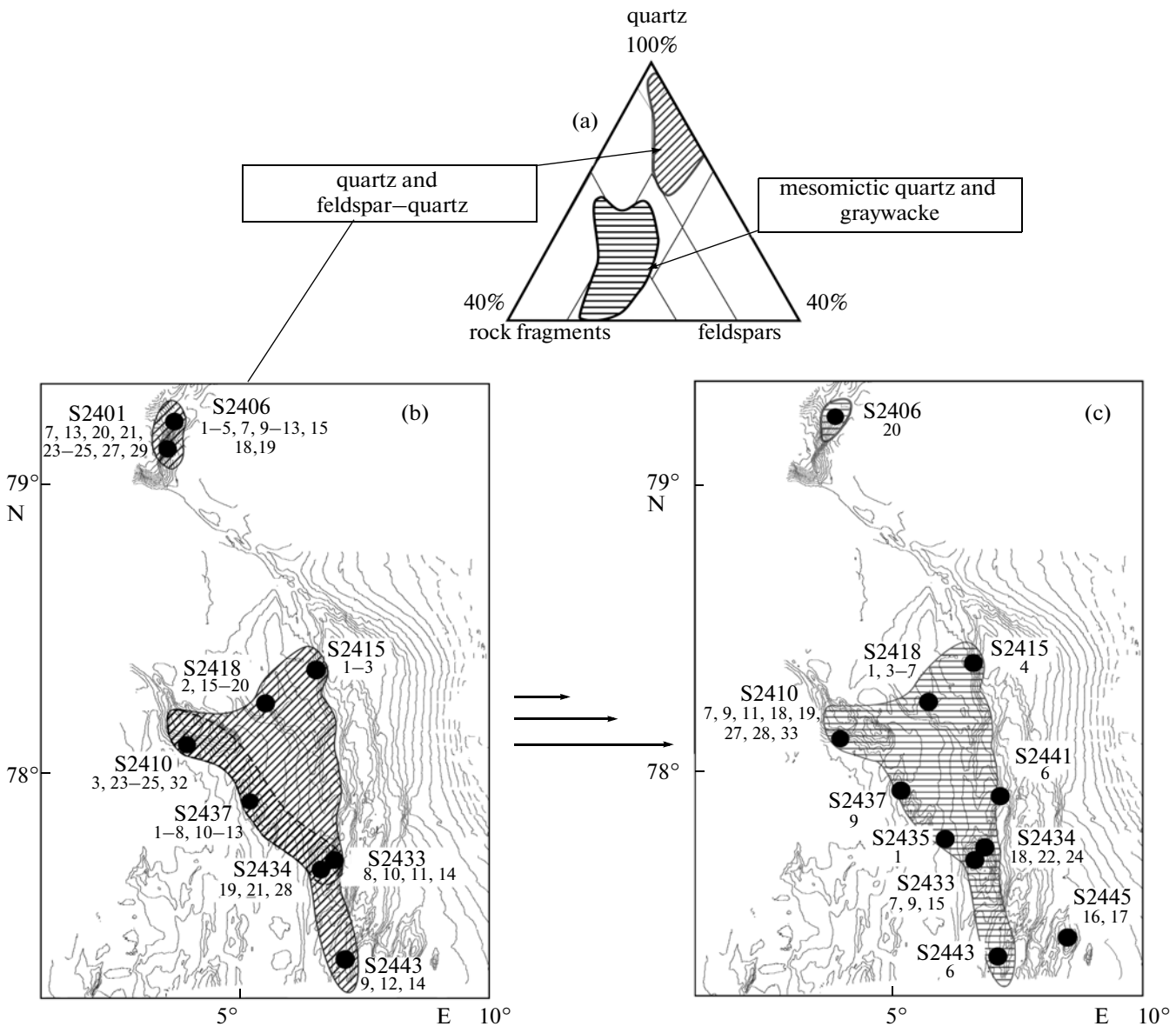

Fig. 6. Distribution of the terrigenous mineral associations in sandstones over the study area. (a) Position of fields of the terrigenous mineral associations in the diagram by (Shutov, 1975); (b, c) distribution of sandstone associations over the study area: (b) feldspar–quartz (dashed line shows the distribution of calcareous varieties), (c) mesomictic quartz–graywacke.

Feldspar–Quartz Sandstones

These rocks are widespread in the Molloy Deep (samples S2401/7, 13, 20, 21, 23–25, 27, 29; S2406/1—5, 7, 9–13, 15, 18, 19), on the western slope of the Knipovich Rift (samples S2415/1–3; S2443/ 9, 12, 14), Svyatogor Rise (samples S2418/2, 15–20), Hovgard Ridge (samples 2410/3, 23–25, 32), Gorynych Hills (samples S2437/1–8, 10–13), and Litvin Seamount (samples S2433/8, 10, 11, 14; S2434/19, 21, 28) (Fig. 6b).

The sandstones are light gray to gay, medium- to fine-grained, less commonly inequigranular, slightly micaceous, locally with pudding pebbles, slightly clayey to clayey, frequently silty and calcareous. Detrital material is subrounded to well-rounded. The rocks contain small inclusions of carbonaceous material. The structure is massive or obscurely bedded (foliated in the strongly altered varieties).

The main share of rocks is composed of clastogenic quartz (largely metamorphogenic or granitoid). Crystalloclasts are represented by plagioclases (up to 20%) with single K-feldspar grains. Lithoclasts (in some samples) of cherts and rare silicified algal limestones constitute up to 10% of the rock (Figs. 5a–5f).

Cement in the low-clay sandstones has the quartzose composition of the regeneration type related to the pressure dissolution of quartz grains. In some

cases, the cement is interstitial or interstitial-basal, clayey, chloritic–hydromicaceous. Some pores are filled with kaolinite. The textural and compositional features allow these rocks to be interpreted as terrigenous.

Some samples from the Hovgard Ridge, Gorynych Hills, and Litvin Seamount exhibit calcite cement and glauconite grains, which imply marine sedimentation settings. Noteworthy is the linear arrangement of sampling points of rocks with such characteristics: samples S2410/3, 32; S2437/1, 5–8; S2433/10, 11, 14; S2434/21, 28 (Fig. 6b).

Postsedimentary alterations of feldspar–quartz sandstones correspond to the stage of deep catagenesis with characteristic conform-regeneration textures of pressure dissolution, locally with microstyloliths. Some sandstone samples dredged from the Hovgard Ridge, Svyatogor Rise, and western slope of the rift valley display recrystallization-granulation blastesis, although the initial detrital texture is preserved (samples S2410/25, S2418/17, S2415/3). In the Molloy Deep, dredging yielded sandstones saturated with thin quartz–chlorite and quartz veinlets characteristic of hydrothermal alteration of rocks.

Mesomictic Quartz–Graywacke Sandstones

These rocks are distributed through the Svyatogor Rise (samples S2418/1, 3–7), Hovgard Ridge (samples S2410/7, 9, 11, 18, 19, 27, 28, 33), Gorynych Hills (sample S2437/9), and Litvin Seamount (samples S24337, 9, 15; S2434/18, 22, 24; S2435/1). Their single samples were taken from the western slope of the rift valley (samples S2415/4, S2441/6, S2443/6) and Molloy Deep (sample S2406/20) (Fig. 6c).

The sandstones are dark gray to greenish gray, fine- to medium-grained, medium-grained, and inequigranular, locally silty, clayey, and frequently calcareous. There are inclusions of carbonaceous matter. Clasts are subangular or subrounded. Some quartz grains are well rounded. The structure is massive, horizontally laminated, or cross-bedded. Slump structures are observed in some places.

Crystalloclasts are represented by quartz (65–40%) and plagioclases (5–20%) Figs. 5b–5f). Lithoclasts are cherts and feldspar–quartz sandstones. There are also intraclasts of silty–clayey rocks. The sandstones contain micas (10%) and glauconite. Sandstones dredged from the Hovgard Ridge (samples S2410/7, 9, 11, 118, 27, 33), Litvin Seamount (samples S2433/7, 9), and western wall of the rift valley (samples S2415/4; S2441/6) contain fragments of altered basalts and chloritized hyaloclastiites. In sediments from the Gorynych Hills (samples S2434/22, 24), more than one-half of rock fragments is represented by altered basalts. Cement in sandstones is clayey interstitial and basal-interstitial chloritic–hydromicaceous, locally calcitic.

Postsedimentary alterations of mesomictic quartz and graywacke sandstones correspond to the stage of deep-seated catagenesis. Varieties with the least clay content demonstrate conform-regeneration textures of pressure dissolution. These rocks from the Molloy Deep are crosscut by abundant quartz–chlorite and quartz veinlets likely related to hydrothermal activity in the study area (sample S2406/20).

DISCUSSION

Insight into the Formation and Development Trend of the Regional Structure

The results of bathymetric studies of the study region suggest that the formation of its structural patterns was governed by two main (NNW- and NNE-oriented) strain systems. The northwestern system includes structures nearly parallel to the strike of the Paleo-Spitsbergen shear zone (approximately 335°). The northeastern orientation (approximately 25°) is characteristic of many fractures traced through the entire region in question, faults crosscutting the Knipovich Rift valley included.

Our original data are consistent with the structural development model of the Greenland and Scandinavian passive margins of the North Atlantic based on the analysis of offshore and onshore materials (Mosar et al., 2002). According to this model, significant structural reorganization in the area, which is located at the divergent boundary between the Greenland and Norwegian margins, took place at the Cretaceous–Paleogene transition. For example, rifting proceeded in the WSW–ENE (up to the latitudinal) direction in the Late Permian–Late Cretaceous, while extension was oriented in the NNW–SSE direction in the Late Cretaceous–Early Tertiary.

It is remarkable that the strike of the NNE-trending fracture system coincides with magnetic anomaly lines defined in the Norwegian–Greenland Basin (Olesen et al., 1997; Mosar et al., 2002), This system includes the Molloy spreading ridge and paleospreading axis between the Knipovich Rift valley and Borei Basin reconstructed near Anomaly 7 (Mosar et al., 2002). In contrast, the NNW-oriented fracture system is parallel to the Senja, Molloy, and Spitsbergen faults, along which adjoining segments of the oceanic crusts are displaced relative to each other.

In this connection, of particular interest is the near-meridional strike of the Knipovich Rift valley. The nature of this structure is debatable, because it displays distinct features of riftogenic oceanic volcanism, on the one hand, and its structure and geophysical fields are inconsistent with their counterparts in the typical well-known mid-oceanic ridges, on the other hand (Gusev and Shkarubo, 2001).

At present, this structure is considered as a spreading ridge (Talwani and Eldholm, 1977; Baturin, 1990; Okino et al., 2002; Shipilov, 2004; Shipilov et al., 2006) or oblique transform rift (Vogt, 198; Thiede et al., 1990; Vogt et al., 1998), transtensional shear sys-

tem (Mosar et al., 2002), shear zone above the gentle detachment surface (Crane et al., 2001), or oceanic rift at the structural arrangement stage (Gusev and Shkarubo, 2001).

As a whole, the structural patterns of the region indicate an influence of shear processes on the formation of the Knipovich Rift (Zaionchek et al., 2007, 2010; Peive and Chamov, 2008; Peive, 2009). The en echelon arrangement of basins of the pull-apart type mapped by the bathymetric survey is characteristic of continental rifts formed by the simple shear mechanism. In addition, the principal difference of the Knipovich Ridge structure from mid-oceanic ridges consists in the lack of significant displacements of rift valley segments along transverse faults and sharp inconsistency between strikes of the structure and linear magnetic anomalies (Olesen et al., 2997; Mosar et al., 2002). The latter circumstance implies young age of the rift. Gusev and Shkarubo (2001) assumed that the present-day rift zone of the Knipovich Ridge resulted from the jump of the spreading axis in the eastern direction in the late Miocene. Moreover, a new extension axis strived for maximal straightening of its strike.

The latter assumption needs additional discussion. The assumed eastward jump of the spreading axis resulted in change in the spatial position of the rift valley and its strike from the SSE direction for the meridional one. Taking into consideration the above-mentioned data on the atypical structure of the Knipovich Ridge and its discordant position relative to magnetic anomalies (direction of the Norwegian–Greenland Basin opening), such a succession of events is hardly probable. Abandonment of the paleospreading ridge after the appearance of shear structure in the terminal Miocene, which became the most optimal tectonic transfer of tectonic strains at least in the northern segment of the Knipovich Ridge, seems to be a more realistic scenario.

The available data are well consistent with the model of the Knipovich Ridge development as a transtensional shear zone, which straightened one (Mosar et al., 2002) or several (Sokolov, 2010) spreading segments of the pre-Miocene oceanic crust. The appearance of such internal shears, which compensated local differences in velocities and directions of deformations in common extension domains, is the simplest solution of the system of tectonic strains (Tevelev, 2005).

It should be noted that kinematic equilibration of strains in the region was also in progress after the Knipovich Rift formation. Our bathymetric data suggest continuation of a system of Knipovich meridional fractures north of the Molloy Fracture Zone (Figs. 1, 2). Crain et al. (2001) arrived at the similar conclusion based on the analysis of SeaMARK II images superposed on the bathymetric survey data.

North of the fracture zone, meridional fractures grade into structures of the Vestnes Ridge, where the strained state of the medium is emphasized by the development of characteristic bottom relief depressions as pockmarks related to gas seeps (Vanneste et al., 2005). The positive relief resembling a central-type volcano is defined east of these factures on the Western Spitsbergen slope in the field of bottom simulating reflectors (Chamov et al., 2008). In the southern area, the sonar survey revealed craters likely related to the subsidence of some areas with the concentrated discharge of gas-saturated fluids (Fig. 2).

The facts presented above suggest that progradation of the Knipovich Transform Zone can continue northward and provoke abandonment of the short Molloy spreading ridge and its withdrawal from the influence of the shear deformation zone. Consequently, the Knipovich Rift as a tectonic transfer will unite the Mohn and Gakkel spreading systems.

In relation to the Molloy Deep isolated from the main morphostructures of the study area, the following working hypothesis may be proposed. In terms of origin, the Molloy Deep belongs to nodal bottom depressions. It represents the characteristic type of structures located at the junction of large fault zones and mid-oceanic ridges. Such depressions were first discovered in the Atlantis and Oceanographer faults, as well as the Gord and Carlsberg ridges (Mazarovich, 2000). Extensive recent data indicate the spatial confinement of nodal depressions to domains with tectonic erosion and exposed rocks of the oceanic crust ("oceanic core complexes"). The best-studied oceanic core complex is located at the eastern intersection of the Mid-Atlantic Ridge with the Atlantis Fracture Zone (30°10′N, 40°05′W) and is structurally associated with the nodal depression (Cann et al., 1997; Blackmann et al., 1998, 2002; Schroeder et al., 2001).

Based on the wide development of extension in the region, spatial position of the Molloy Deep, and discovery of ultramafic rocks on its slope, we may assume its relations with the tectonic exhumation of deep crustal layers.

The oceanic core complexes represent analogues of metamorphic core complexes that are widespread on continents and serve as indicator of large-scale crustal extension in line with the simple shear mechanism (Coney, 1980; Coney and Harms, 1984; Lister and Davis, 1989; Buck, 1991; Sklyarov et al., 1997). Recognition of such structures may contribute much to understanding of the structure and development trend of the region.

Relationship and Age of Seismocomplexes

A great number of seismostratigraphic schemes are available for the sedimentary cover of the Norwegian–Greenland Basin (Hinz and Schluter, 1978; Baturin, 1986, 1992; Savostin and Baturin, 1986; Faleide et al., 1996; Shkarubo, 1999). The most recent scheme is proposed in (Gusev and Shkarubo, 2001), which is based on the analysis of multichannel seismic profiling

records and takes into account materials of deep-sea drilling in the Fram Strait.

Based on seismic record patterns, deformations (degree and character) of sedimentary sequences, relations of complexes between each other and with the acoustic basement, the latter authors defined four large seismostratigraphic units. The Miocene–Quaternary complex is developed on the continental slope and in the Knipovich Rift valley, while the remainder of the region is occupied by the Oligocene, Miocene, and Miocene seismocomplexes. The young units occupy a structurally higher position and virtually always rest upon the Oligocene seismocomplex, which is mapped in isolated depressions, on terraces, and in "pockets."

These researchers revealed a westward thinning of seismocomplexes, suggesting the transport of sediments from the Spitsbergen margin through the present-day Knipovich Rift valley, which was shallower or missing at all at that time. The young age of the rift valley is also evident from the following observations: the chain of the highest summits of the ridge crest correlates with the magnetic Anomaly 3 (Shkarubo, 1996; Gusev and Shkarubo, 2001).

Seismocomplexes defined in the CSP and VAP records are well consistent with the above-mentioned observations. For example, we united all sediments of the continental slope and rift valley into a single Seismocomplex A, since it is characterized by a distinct morphological confinement and its whole section cannot be studied by the available methods. Its age is estimated as the Miocene–Holocene. Its upper (finely stratified) part is most likely analogous to Seismocomplex B.

Based on correlation with ODP holes drilled on the Hovgard Ridge, where they penetrated Quaternary sediments to a depth of approximately 100 m (Thiede et al., 1995), seismocomplex B is estimated as the Pliocene–Holocene in age.

The most reliable age estimate was likely obtained for Seismocomplex C. Upper Miocene sediments were recovered from the depth interval of 100–200 mbsf on the Hovgard Ridge and 150–300 mbsf in the Fram Strait. In both areas, they are underlain by Oligocene–lower Miocene sediments that are observed sown to a depth of approximately 400 m (Thiede et al., 1995). Taking into consideration these data and position of the basal intense reflector on the Svyatogor Rise, Seismocomplex C may be attributed to the Miocene.

According to our seismostratigraphic subdivision of the sedimentary cover, all pre-Miocene sediments are referred to Seismocomplex D. Let us recollect that deep-sea drilling recovered Oligocene sediments at a depth of about 400 mbsf (Thiede et al., 1995). Gusev and Shkarubo (2001) also consider the lower seismocomplex as the Oligocene in age. Our analysis of agglutinate benthic foraminifers suggest that Seismocomplex D includes sediments deposited in the Late Paleocene–middle Eocene.

Thus, seismic complexes defined in this work based on their distribution, position in the sedimentary section, and age estimates correlate with the seismostratigraphic units proposed in (Gusev and Shkarubo, 2001). The most significant inconsistency in age estimates concerns Seismocomplex D. It should be emphasized that further detailed investigations are needed for specifying the boundaries and spatial distribution of these seismocomplexes, as well as for dating the seismostratigraphic bodies with different wave field patterns.

Relationship between Lithogenetic Complexes and Their Sedimentation Settings

The composition of rock-forming components in sandstones suggests a directed temporal succession of terrigenous mineral associations from the feldspar–quartz to mesomictic quartz–graywacke one. Moreover, it displays a distinct compositional inheritance of associations, when the newly formed terrigenous mineral complex partly becomes a source for the next one. The inheritance of detrital material sources allows one to consider the contrasting complexes of sandy rocks as elements of a single stratigraphic section.

Quartz and feldspar–quartz sandstones are presumably fluvial and fluvial–deltaic in origin. The coastal-marine settings were likely developed in the area of the present-day Hovgard Ridge, Gorynych Hills, and Litvin Seamount.

This assumption is consistent with the data on Paleogene diatom assemblages from ODP Hole 908 drilled in the aseismic Hovgard Ridge, which are characteristic of the neritic and coastal settings with low-salinity waters (Gusev and Shkarubo, 2001). They also include freshwater acidophilic representatives of the genera *Eunotia* and *Pinnularia*, suggesting the development of coastal swamps and marches at that time (Scherer and Kocc, 1996).

The older sandy sequences or weathered crystalline rocks of platform basement served as the main source of sedimentary material. An insignificant share of detrital material originated from the eroded siliceous sequences.

The mesomictic quartz and graywacke sandstones accumulated in high-energy hydrodynamic marine settings under the influence of waves and bottom currents. Detrital material was transported from the same sources, which supplied also it during accumulation of the quartz–feldspar sequence. The latter also served as a source of material. At the same time, the presence of altered volcaniclastics suggests a new additional source, which supplied the detrital volcanogenic basic material into the sedimentation basin.

The appearance of volcanogenic material indicates tectonic activation of the region and intensified differ-

entiation of the basin bottom. This was accompanied by the local uplifting and exhumation of basic rocks, such as basalts of the Pogrebitskii Seamount (samples S2445/16, 17) (Gusev and Shkarubo, 2001).

In terms of lithostructural features, fluvial-deltaic and coastal-marine feldspar–quartz sandstones represent fragments of older parts of the sedimentary section. The mesomictic quartz and graywacke sandstones of marine genesis are elements of the overlying younger sequence, which was forming in tectonically active settings after the hiatus, partial erosion of the underlying feldspar–quartz sediments, and formation of new intrabasin sources of detrital material.

Different degrees of postsedimentary alteration in sandstones even within a single association indicate different thermobaric conditions in the study region. Hence, depending on the tectonic setting, the rocks selectively experienced, in addition to lithostatic load, the thermodynamic impact likely related to rifting.

As a whole, progressive decrease in the mineralogical maturity of sandstones during the replacement of continental sedimentation settings by marine conditions reflects the general destruction of continental crust during its extension up to the point of formation of the oceanic crust.

CONCLUSIONS

The presented data provide grounds for several inferences and assumptions, which should be tested and specified by further studies. The main results of the performed study are as follow.

Bathymetric survey of the bottom surface by the multibeam echo sounder coupled with the continuous seismic and vertical acoustic profiling revealed two main (NNW- and NNE-trending) fracture systems in the present-day tectonic structure of the study region. The NNE-oriented fracture system, linear zones of the predominance of keyboard deformations included, are consistent with the strike of the reconstructed linear magnetic anomalies.

Analysis of tectonic structure of the Knipovich Ridge confirms its formation as a transtensional shear zone that straightened one (Mosar et al., 2002) or several (Sokolov, 2010) spreading segments of the pre-Miocene oceanic crust. It is assumed that the northward progradation of the Knipovich Transform Zone should provoke abandonment of the short Molloy spreading ridge, its withdrawal from the influence of the shear deformation zone, and transformation of the Knipovich Ridge into a tectonic transfer, which will unite the Mohn and Gakkel spreading systems.

According to the proposed working hypothesis, the Molloy Deep is related to the paragenesis of structures characteristic of core oceanic complexes that are widespread near intersections of transform faults and spreading ridges.

According to wave field patterns in CSP records, the sedimentary cover of the study region comprises four seismocomplexes that indicate contrasting sedimentation settings and intense tectonic processes at different formation stages of the northern Norwegian–Greenland Basin.

It is established that the Molloy Fracture Zone is responsible for the appearance of a horizontal reflector system represented by transparent structureless light spots ("blankings") characteristic of areas with ascending pore fluids.

The study of microfossils revealed a wide development of Miocene palynomorphs, planktonic foraminifers, and diatoms accompanied by upper Paleocene–middle Eocene benthic foraminifers.

The composition of rock-forming components in sandstones indicates a directed temporal succession of terrigenous mineral associations from the feldspar–quartz to mesomictic quartz–graywacke one. Progressive decrease in the mineralogical maturity of sandstones in the course of the presumed replacement of continental setting by marine sedimentation reflects a general trend of continental crust destruction during its extension up to the formation of the oceanic crust.

Further investigations should include the following main tasks.

The defined seismocomplexes should be traced through the study region. The obtained facies maps of seismocomplexes will serve as a basis for the correlation of sediments and selection of dredging sites for sampling the sedimentary cover in areas most suitable for the solution of stratigraphic problems.

Special attention should be paid to the study of the Molloy Deep slopes. In particular, the SeaBat hydroacoustic complex should be used for the search of the mullion structures, i.e., characteristic structures related to exhumation of the detachment surface during the formation of the core oceanic complexes. Another object deserving the thorough bathymetric mapping is an area of the presumed continuation of meridional factures of the Knipovich Rift north of the Molloy Fracture Zone.

ACKNOWLEDGMENTS

We are grateful to the crew of the R/V *Akademik Nikolaj Strakhov* for the invaluable help in field investigations. We also thank M.J. Head (Brock University, Ontario, Canada) and A.O. Mazarovich (GIN RAN) for consultation.

This work was supported by the Norwegian Petroleum Directorate, Presidium of the Russian Academy of Sciences (program nos. 14, 16, and 17), program for the support of leading scientific schools (project nos. NSh-9664.2006.5, academician Yu.M. Pushcharovsky, supervisor; NSh-5508.2008.5, Academician Yu.G. Leonov, supervisor), and Russian Foundation for Basic Research (project no. 09-05-00150).

REFERENCES

Baturin, D.G., The Western Continental Margin of the Spitsbergen Archipelago, Tectonics, and Sedimentation, in *Geologiya osadochnogo chekhla Shpitsbergena* (Geology of the Sedimentary Cover of Spitsbergen), St. Petersburg: PGO Sevmorgeologiya, 1986, pp. 126–135.

Baturin, D.G., Structure and Geodynamics of the Molloy Transform Fracture Zones in the Mid-Ridge System of the Norway–Greenland Oceanic Basin, *Okeanologiya*, 1990, vol. 30, no. 3, pp. 436–443.

Baturin, D.G., Seismostratigraphy of Sedimentary Basins at the West Spitsbergen Continental Margin, *Otechest. Geol.*, 1992, no. 10, pp. 67–74.

Blackman, D.K., Cann, J.R., Janssen, B., and Smith, D.K., Origin of Extensional Core Complexes: Evidence from the Mid-Atlantic Ridge at Atlantis Fracture Zone, *J. Geophys. Res.*, 1998, vol. 103 (21), pp. 21315–21334.

Blackman, D.K., Karson, J.A., Kelley, D.S., et al., Geology of the Atlantis Massif (Mid-Atlantic Ridge, 30°N): Implications for the Evolution of an Ultramafic Oceanic Core Complex, *Mar. Geophys. Res.*, 23, 2002, pp. 443–469.

Bolli, H.M. and Saunders, J.B., Oligocene to Holocene Low Latitude Planktic Forammifera, *Plankton Stratigraphy,* Cambr. Univ. Press, 1985, pp. 155–262.

Boltovskoy, A., Watanabe, S., Totah, V.I., Vera Ocampo, J., Cenozoic Benthic Bathyal Foraminifers of DSDP Site 548 (North Atlantic), *Micropaleontology,* 1992, vol. 38 no. 2, pp. 183–207.

Braathen, A., Osmundsen, P.T., Nordgulen, Ø., et al., Orogen-Parallel Extension of the Caledonides in Northern Central Norway: An Overview, *Norweg. J. Geol.*, 2002, vol. 82, pp. 225–241.

Brekke, H., *The Tectonic Evolution of the Norwegian Sea Continental Margin with Emphasis on the Vöring and Möre Basins*, Geol. Soc. London. Spec. Publ., 2000, vol. 167, pp. 327–378.

Brekke, H., Sjulstad, H.I., Magnus, C., and Williams, R.W., Sedimentary Environments Offshore Norway—An Overview, Sedimentary Environments Offshore Norway—Palaeozoic to Recent, *NPF Spec. Publ.*, Amsterdam: Elsevier, 2001, vol. 10, pp. 7–37.

Buck, W.R., Modes of Continental Lithospheric Extension, *J. Geophys. Res.*, 1991, vol. 96, pp. 20161–20178.

Cann, J.R., Blackman, D.K., Smith, D.K., et al., Corrugated Slip Surfaces Formed at Ridge-Transform Intersections on the Mid-Atlantic Ridge, *Nature,* 1997, vol. 385, pp. 329–332.

Chamov, N.P., Dobrolyubova, K.O., Peive, A.A., and Sokolov, S.Yu., Signs of the Presence of Gas Hydrates in the Upper Portion of the Sedimentary Cover at Flanks of the Molloy Fracture Zone (Fram Strait, Norway–Greenland Basin), *Byull. MOIP. Ser. Geol*, 2008, no. 2, pp. 51–60.

Coney, P.J., Cordilleran Metamorphic Core Complexes, *Geol. Soc. Am. Mem.*, 1980, vol. 153, pp. 7–34.

Coney P.J., Harms T.A. Cordilleran Metamorphic Complexes: Cenozoic Relics of Mesozoic Compression, *Geology,* 1984, vol. 12, pp. 550–554.

Crane, K., Doss, S., Vogt, P., et al., The Role of the Spitsbergen Shear Zone in Determining Morphology, Segmentation and Evolution of the Knipovich Ridge, *Mar. Geophys. Res.*, 2001, vol. 22, pp. 153–205.

De Verteuil, L. and Norris, G., Dinoflagellate Cyst Zonation and Allostratigraphy of the Chesapeake Group, *Miocene Dinoflagellate Stratigraphy and Systematics of Maryland and Virginia Micropaleontology*, 1996, vol. 42, pp. 1–172.

Doré, A.G., Lundin, E.R., Birkeland, Ø., et al., Principal Tectonic Events in the Evolution of the Northwest European Atlantic Margin, *Petroleum Geology of NW Europe, Proc. 5th Conf.*, London: Geol. Soc., 1999, pp. 41–61.

Dynamics of the Norwegian Margin, Nøttvedt, A., et al., Eds., London: Geol. Soc. Spec. Publ., 2000, vol. 167.

Efimov, V.N., *Seismic Air-Operated Wave Transducer*, RF Patent No. 2377603 (2008).

Eide, E.A., Osmundsen, P.T., Meyer, G.B., et al., The Nesna Shear Zone, North-Central Norway: An 40Ar/39Ar Record of Early Devonian-Early Carboniferous Ductile Extension and Unroofing, *Norweg. J. Geol.*, 2002, vol. 82, pp. 317–339.

Faleide, J. I., Solheim, A., Fiedler, A., et al., Late Cenozoic Evolution of the Western Barents Sea - Svalbard Continental Margin, *Global Planet. Change*, 1996, vol. 12, pp. 53–74.

Fleet A.J. and Boldy, S.A.R., Petroleum Geology of Northwest Europe, *The Fifth Conference of the Petroleum Geology of Northwest Europe*, London: Geol. Soc., 1999, no. 1398.

Ginsburg, G.D. and Solov'ev, V.A., *Submarinnye gazovye gidraty* (Submarine Gas Hydrates), St. Petersburg: VNIIOkeangeologiya, 1994.

Gusev, E.A. and Shkarubo, S.I., Anomalous Structure of the Knipovich Ridge, *Russ. J. Earth Sci*, 2001, vol. 3 (2), pp. 145–161.

Gradstein, P.M. and Kaminski, M.A., Taxonomy and Biostratigraphy of New and Emended Species of Cenozoic Deep-Water Agglutinated Foraminifera from the Labrador and North Sea, *Micropaleontology*, 1989, vol. 35 (1), pp. 72–92.

Gradstein, P.M., Kaminski, M.A., Berggren, W.A., et al., Cenozoic Biostratigraphy of the North Sea and Labrador Shelf, *Micropaleontology*, 1994, Supp., vol. 40, pp. 1–152.

Gusev, E.A., Issue of the Spitsbergen Continental Margin, in *Tektonika i geodinamika: obshchie i regional'nye aspekty* (Tectonics and Geodynamics: General and Regional Aspects), Moscow: GEOS, 1999, pp. 229–232.

Gusev, E.A., Oligocene Stage of the Tectonic Development of the Greenland Sea, in *Kompleksnye issledovaniya prirody Shpitsbergena* (Complex Investigations of the Nature of Spitsbergen), Apatity: KNTs RAN, 2005, vol. 5, pp. 157–167.

Hansen, H.-E., Amundsen, H. E. F., Snow, J. E., Pedersen, R. B., A Comparison of Peridotites from the Molloy Deep and the Gakkel Ridge with Mantle Xenoliths from Spitsbergen., *Geophys. Res. Abstr.*, 2003, vol. 5, no. 13638.

Hartz, E. H., Eide, E. A., Andresen, E. A., et al., 40Ar/39Ar Geochronology and Structural Analysis: Basin Evolution and Detrital Feedback Mechanisms, Hold with Hope Region, East Greenland, *Norweg. J. Geol.*, 2002, vol. 82, pp. 341–358.

Head, M.J., Norris, G., and Mudie, P.J., Palynology and Dinocyst Stratigraphy of the Miocene in ODP Leg 105, Hole 645E, Baffin Bay, *Proc. ODP, Sci. Res.*, 1989, pp. 467–514.

Hinz, K. and Schluter, H.-U., The Geological Structure of the Western Barents Sea, *Mar. Geol.*, 1978, vol. 26, pp. 199–230.

Hulsbos, R.E., Kroon, D., Jansen, H.S.M., and van Hinte, J.E., Lower Eocene Benthic Foraminifera and Paleoenvironment of the Outer Vöring Plateau, Norwegian Sea (DSDP Site 338), *Micropaleontology*, 1989, vol. 35 (3), pp. 256–273.

Lister, G.S. and Davis, G.A., The Origin of Metamorphic Complexes and Detachment Faults Formed during Tertiary Continental Extension in the Northern Colorado River Region, U.S.A., *J. Struct. Geol.*, 1989, vol. 11, pp. 65–94.

Lundin, E.R. and Doré, A.G., A Tectonic Model for the Norwegian Passive Margin with Implications for the NE Atlantic: Early Cretaceous to Break-Up, *J. Geol. Soc.*, London, 1997, vol. 154, pp. 545–550.

Miller, K.G., Gradstern, P.M., and Berggren, W.A., Late Cretaceous to Early Tertiary Agglutinated Benthic Foraminifera in the Labrador Sea, *Micropaleontology*, 1982, vol. 28, no. 1, pp. 1–30.

Mazarovich, A.O., *Kratkii tolkovyi slovar anglo- i russkoyazychnykh terminov po tektonike i geomorfologii okeana* (Concise Explanatory Dictionary of English and Russian Terms in Tectonics and Geomorphology of Ocean), Moscow: Nauchnyi Mir, 2000.

Mosar, J., Eide, E.A., Osmundsen, P.T., et al., Greenland-Norway Separation. A Geodynamic Model for the North Atlantic, *Norweg. J. Geol.*, 2002, vol. 82, pp. 281–298.

Mudie, P.J., Palynology and Dinoflagellate Biostratigraphy of Deep Sea Drilling Project Leg 94, Sites 607 and 611, North Atlantic Ocean, *Proc. DSDP, Init. Rep.*, Washington, DC, 1987, vol. 94, pp. 785–812.

Mudie, P.J., Palynology and Dinocyst Biostratigraphy of the Late Miocene to Pleistocene, Norwegian Sea; ODP Leg 104, Sites 642 and 644., *Proc. ODP, Sci. Res.*, 1989, vol. 104, pp. 587–610.

Myhre, A. M., Eldholm, O., and Sundvor, E., The Margin between the Senja and Spitsbergen Fracture Zones: Implications from Plate Tectonics, *Tectonophysics*, 1982, vol. 89, pp. 33–50.

Nagy, J., Kaminski, M.A., Johnsen, K., and Vitlehnner, A.C., Foraminiferal, Palinomorph, and Diatom Biostratigraphy and Paleoenvironments of the Torsk Formation: A Reference Section for the Paleocene-Eocene Transition in the Western Barents Sea, *Grzybowski Foundation Spec. Publ.*, 1997, vol. 5, pp. 15–38.

Nagy, J., Kaminski, M.A., Kuhnt, W., and Bremer, M.A., Agglutinated Foraminifera from Neritic to Bathyal Facies in the Palaeogene of Spitsbergen and the Barents Sea, *Proc. Fifth Int. Workshop on Agglutinated Foraminifera*, Grzybowski Foundation Spec. Publ., 2000, vol. 7, pp. 333–361.

Okino, K., Curewitz, D., Asada, M., et al., Preliminary Analysis of the Knipovich Ridge Segmentation: Influence of Focused Magmatism and Ridge Obliquity on an Ultraslow Spreading System, *Earth Planet. Sci. Lett.*, 2002, vol. 202, pp. 275–288.

Olesen, O.G., Gellein, J., Habrekke, H., et al., *Magnetic Anomaly Map, Norway and Adjacent Ocean Areas, Scale 1 : 3 Million*, Geol. Surv. Norway, 1997.

Osmundsen, P.T., Sommaruga, A., Skilbrei, J.R., and Olesen O., Deep Structure of the Norwegian Sea Area, North Atlantic Margin, *Norweg. J. Geol.*, 2002, vol. 82, pp. 205–224.

Osmundsen, P.T., Braathen, A., Nordgulen, O., et al., The Devonian Nesna Shear Zone and Adjacent Gneiss-Cored Culminations, North-Central Norwegian Caledonides, *J. Geol. Soc. London*, 2003, vol. 160, pp. 1–14.

Parker, J.R., Petroleum Geology of Northwest Europe, *The Fourth Conference of the Petroleum Geology of Northwest Europe*, London: Geol. Soc., 1993, no. 1542.

Peive, A.A. and Chamov, N.P., Main Features of the Tectonics of the Knipovich Ridge (North Atlantic) and History of Its Evolution at the Neotectonic Stage, *Geotektonika*, 2008, no. 1, pp. 38–57 [*Geotectonics* (Engl. Transl.), 2008, no. 1, pp. 31–47].

Peive, A.A., Accretion of the Continental Crust during Oblique Spreading, *Geotektonika*, 2009, no. 2, pp. 5–19 [*Geotectonics* (Engl. Transl.), 2009, no. 2, pp. 3–15].

Poulsen, N.E., Manum, S.B., Williams, G.L., and Ellegaard, M., Tertiary Dinoflagellate Biostratigraphy of Sites 907, 908, and 909 in Norwegian-Greenland Sea, *Proc. ODP, Sci. Res.*, 1996, vol. 151, pp. 255–287.

Sokolov, S.Yu., Efimov, V.N., Mazarovich, A.O., et al., Structure of the Sedimentary Cover in the Western African–Antarctic Ridge (Southern Atlantic), *Dokl. Akad. Nauk*, 1999, vol. 366, no. 2, pp. 231–235 [*Dokl. Earth Sci.* (Engl. Transl.), 1999, vol. 366, no. 2, pp. 215–218].

Savostin, L. A. and Karasik, A.M., Recent Plate Tectonics of the Arctic Basin and of the Northeastern Asia., *Tectonophysics*, 1981, vol. 74, pp. 111–145.

Scherer, R.D. and Kocc, N., Late Paleogene Diatom Biostratigraphy and Paleoenvironments of the Northern Norwegian-Greenland Sea, *Proc. ODP, Sci. Res.*, 1996, vol. 151, pp. 75–78.

Savostin, L.A. and Baturin, D.G., Seismostratigraphy and Cenozoic History of the Continental Crust of the Greenland Sea at the Southern End of the Spitsbergen Archipelago, *Dokl. Akad. Nauk SSSR*, 1986, no. 291 (6), pp. 1458–1462.

Schroeder, T., John, B.E., Kelley, D., et al., Microstructural Observations of an 'Oceanic Core Complex': Atlantis Massif, 30°N Mid-Atlantic Ridge, *EOS Trans. AGU,* 2001, vol. 82, F1100.

Skogseid, J., Planke, S., Faleide, J.I., Pedersen, T., Eldholm, O., and Neverdal, F., NE Atlantic Continental Rifting and Volcanic Margin Formation, *Geol. Soc. London, Spec. Publ.*, 2000, vol. 1, pp. 295–326.

Shipilov, E.V., Tectonic–Geodynamic Evolution of Continental Margins of the Arctic during Epochs Young Ocean Formation, *Geotektonika*, 2004, no. 5, pp. 26–52 [*Geotectonics* (Engl. Transl.), 2004, no. 5, pp. 21–45].

Shipilov, E.V., Shkarubo, S.I., and Raznitsin, Yu.N., Neotectonics of the Northern Norway–Greenland Basin (Specific Features of the Structure and Development of the Knipovich Ridge and Pomor'e Perioceanic Trough), *Dokl. Akad. Nauk*, 2006, vol. 410, no. 4, pp. 506–511 [*Dokl. Earth Sci.* (Engl. Transl.), 2006, vol. 410, no. 4, pp. 475–479].

Shkarubo, S.I., Specific Features of the Spreading in the Northern Norway–Greenland Basin, in *Geologo-geofizicheskie kharakteristiki litosfery Arkticheskogo regiona* (Geological-Geophysical Characteristics of Lithosphere in the Arctic Region), St. Petersburg: VNIIOkeangeologiya, 1996, pp. 101–114.

Shkarubo, S.I., Geodynamic Aspects of the Evolution of the Northern Norway–Greenland Basin, in *25 let na Arkticheskom shel'fe Rossii* (25 Years on the Russian Arctic Shelf), St. Petersburg: VNIIOkeangeologiya, 1999, pp. 71–79.

Shutov, V.D., *Mineral'nye paragenezy grauvakkovykh kompleksov* (Mineral Parageneses of Graywacke Complexes), Moscow: Nauka, 1975.

Sklyarov, E.V., Mazukabzov, A.M., and Mel'nikov, A.I., *Kompleksy metamorficheskikh yader kordil'erskogo tipa* (Complexes of Metamorphic Cores of the Cordillera Type), Novosibirsk: SO RAN, NITs OIGGM, 1997.

Smelror, M., Pliocene–Pleistocene and Redeposited Dinoflagellate Cysts from the Western Svalbard Margin (Site 986): Biostratigraphy, Paleoenvironments, and Sediment Provenance, *Proc. ODP, Sci. Res.*, 1999, vol. 162, pp. 83–97.

Sokolov, S.Yu., Tectonic Evolution of the Knipovich Ridge Based on the Anomalous Magnetic Field, *Dokl. Akad. Nauk* (in press).

Talwani, M. and Eldholm, O., Evolution of the Norwegian-Greenland Sea, *Geol. Soc. Am. Bull.*, 1977, vol. 88, pp. 969–994.

Talwani, M., Udintsev, G., et al., *Proc. DSDP, Init. Rep.*, VI. 38, Washington: U.S. Gov. Printing Office,1976.

Tevelev, A.V., *Sdvigovaya tektonika. Uchebnoe posobie* (Shear Tectonics: Manual), Moscow: Mosk. Gos. Univ., 2005.

Thiede, J., Myhre, A. M., Firth, J.V., et al., Cenozoic Northern Hemisphere Polar and Subpolar Ocean Paleoenvironments (Summary of ODP Leg 151 Drilling Results), *Proc. ODP, Init. Rep.*, 1995, vol. 151, pp. 397–420.

Thiede, J., Pfirman, S., Schenke, H.W., and Reil, W., Bathymetry of Molloy Deep: Fram Strait between Svalbard and Greenland, *Mar. Geophys. Res.*, 1990, vol. 12, pp. 197–214.

Torske, T. and Prestvik, T., Mesozoic Detachment Faulting between Greenland and Norway: Inferences from Jan Mayen Fracture Zone System and Associated Alkalic Volcanic Rocks, *Geology*, 1991, vol. 19, pp. 481–484.

Torsvik, T.H.,Van der Voo, R., Meert, J.G., et al., Reconstructions of Continents around the North Atlantic at about the 60th Parallel, *Earth Planet. Sci. Lett.*, 2001, vol. 187, pp. 55–69.

Valyaev, B.M., Tectonic Control of Oil and Gas Accumulation and Hydrocarbon Degassing of the Earth, in *Teoreticheskie i regional'nye problemy geodinamiki* (Theoretical and Regional Problems of Geodynamics), Moscow: Nauka, 1999, pp. 222–252.

Vanneste, M., Guidard, S., and Mienert J., Bottom Simulating Reflection and Geothermal Gradients across the Western Svalbard Margin, *Terra Nova*, 2005, vol. 17, pp. 510–516.

Vogt, P.R., Geophysical and Geochemical Signatures and Plate Tectonics, *The Nordic Seas*, New York: Springer, 1986, pp. 413–663.

Vogt, P.R., Jung, W.Y., and Brozena, J., Arctic Margin Gravity Highs Remain Puzzle, *EOS. Trans. Am. Geophys. Union*, 1998, vol. 79, pp. 601–606.

Zaionchek, A.V., Brekke, H., Sokolov, S.Yu., et al., Structure of the Continent-Ocean Transition Zone in the Northwestern Framing of the Barents Sea (Based on Cruises 24, 25, and 26 of the R/V *Akademik Nikolai Strakhov*, 2006–2009), in *Rezul'taty issledovaniya Mezhdunarodnogo polyarnogo goda* (Results of the Investigation in the International Polar Year), Moscow: Evrop. Izd., 2010, vol. 4, pp. 107–153.

Ziegler, P.A., Post-Hercynian Plate Reorganization in the Tethys and Arctic North Atlantic Domains, *Triassic-Jurassic Rifting. Developments in Geotectonics*, Amsterdam: Elsevier, 1988, vol. 22, pp. 71–75.

Zaionchek, A.V., Dobrolyubova, K.O., Peive, A.A., et al., New Data on the Structure of the Continental Margin of the Atlantic Ocean West of the Spitsbergen Archipelago, in *Geologiya morei i okeanov* (Geology of Seas and Oceans), Moscow, 2007, vol. 4, pp. 82–84.